
Article:
George, IJ, Matthews, PS, Whalley, LK et al. (2013) Measurements of uptake coefficients for heterogeneous loss of HO2 onto submicron inorganic salt aerosols. Physical Chemistry Chemical Physics, 15 (31). 12829 - 12845. ISSN: 1463-9076

https://doi.org/10.1039/c3cp51831k

Measurements of uptake coefficients for heterogeneous loss of HO_2 onto submicron inorganic salt aerosols

I. J. George[1,2], P. S. J. Matthews[1], L. K. Whalley[1,3], B. Brooks[3,4], A. Goddard[1], M. T. Baeza-Romero[5], D. E. Heard[1,3,#]

[1]*School of Chemistry, University of Leeds, Woodhouse Lane, Leeds, LS2 9JT, UK*
[2]*Now at National Risk Management Research Laboratory, U.S. Environmental Protection Agency, T.W. Alexander Drive, Durham, NC 27709*
[3]*National Centre for Atmospheric Chemistry, University of Leeds, Woodhouse Lane, Leeds, LS2 9JT, UK*
[4]*School of Earth and Environment, University of Leeds, Woodhouse Lane, Leeds, LS2 9JT, UK*
[5]*Escuela de Ingeniería Industrial de Toledo, Universidad de Castilla la Mancha, Toledo, 45071, Spain*

[#]Corresponding author

Abstract

Laboratory studies were conducted to investigate the kinetics of HO_2 radical uptake onto submicron inorganic salt aerosols. HO_2 reactive uptake coefficients were measured at room temperature using an aerosol flow tube and the Fluorescence Assay by Gas Expansion (FAGE) technique that allowed for measurements to be conducted under atmospherically relevant HO_2 concentrations ($[HO_2] = 10^8$ to 10^9 molecule cm^{-3}). The uptake coefficient for HO_2 uptake onto dry inorganic salt aerosols was consistently below the detection limit ($\gamma_{HO2} < 0.004$). The mass accommodation coefficient of HO_2 radicals onto Cu(II)-doped $(NH_4)_2SO_4$ aerosols was measured to be $\alpha_{HO2} = 0.4 \pm 0.3$ representing the kinetic upper limit to γ. For aqueous $(NH_4)_2SO_4$, NaCl and NH_4NO_3 aerosols not containing traces of transition metal ions, a range of $\gamma_{HO2} = 0.003\text{-}0.02$ was measured. These values were much lower than γ values previously measured on aqueous $(NH_4)_2SO_4$ and NaCl aerosols and also those typically used in atmospheric models ($\gamma_{HO2} = 0.1–1.0$). Evidence is presented showing that the HO_2 uptake coefficients onto aqueous salt aerosol particles are dependent both on the exposure time to the aerosol and on the HO_2 concentration used.

1. Introduction

The hydroxyl (OH) and hydroperoxyl (HO_2) radicals ($HO_x \equiv OH + HO_2$) are the key reactive chemical species that control the oxidative capacity of the troposphere. OH radical-initiated oxidation reactions determine the atmospheric lifetimes and concentrations of most trace gases in the troposphere, e.g. NO_x (NO and NO_2), O_3, CH_4 and volatile organic compounds (VOCs). OH reactions with CO and VOCs lead to the production of HO_2 radicals, which are rapidly recycled back to OH through further reactions with NO, O_3 and halogen oxides. HO_2 radical reactions in the troposphere can lead to either O_3 production or destruction depending on NO_x levels. Therefore, the ability to predict the fate of atmospheric pollutants necessitates a detailed knowledge of the sources and sinks of HO_x in order for models to calculate their concentrations.

Over the past few decades, field measurements of atmospheric HO_x concentrations have been compared to calculated levels from a variety of numerical models to evaluate our current understanding of atmospheric photochemistry. In some studies, zero-dimensional (or box) models, incorporating a chemical mechanism for gas-phase photochemistry and constrained by ancillary atmospheric measurements (e.g. O_3, NO_x, VOCs, and photolysis frequencies), have significantly overpredicted field measured HO_2 concentrations[1-15]. For most of these studies, particularly those conducted in the clean marine boundary layer at low NO_x, including heterogeneous uptake of HO_2 onto aerosols in the model was able to improve the level of agreement, but large values of the uptake coefficient, γ_{HO2}, even as high as γ_{HO2}=1, were often used. Subsequent studies in the marine environment recognized the importance of the halogen oxides BrO and IO in removing HO_2[11, 16, 17]. Once this halogen chemistry was included in the chemical mechanism used by models, it was in some cases possible to gain better agreement using smaller values of the HO_2 uptake coefficient, although considerable uncertainty remains. The global impact of heterogeneous loss of HO_2 onto aerosols has been assessed by chemistry transport models[18-21], which demonstrate that heterogeneous HO_2 uptake onto aerosols can significantly reduce tropospheric HO_x concentrations. In these studies, a single and relatively large uptake coefficient of γ_{HO2}=0.2 has been used as recommended by Jacob[22].

The majority of models have used large reactive HO_2 uptake coefficients (γ_{HO2} = 0.1−1.0) to assess the tropospheric impact of HO_2 uptake to aerosols. However, HO_2 uptake coefficients as determined by previous laboratory studies at room temperature are inconsistent and span a wide range of values. Measured HO_2 reactive uptake coefficients reported in the literature are summarized in Table 1 for single component salt surfaces and Cu(II)-doped salts at room temperature. Several experimental methods have been used to determine these values, but relatively few measurements have been conducted with atmospherically relevant HO_2 concentrations ([HO_2] on the order of ~10^8 molecule cm^{-3}) or with aerosol particles rather than solid films. Mozurkewich et al.[23] conducted the first laboratory measurements of HO_2 uptake onto aqueous aerosol particles doped with Cu(II) ions to catalyze the oxidation of HO_2, and hence its removal in the bulk phase. These studies enabled the determination of the mass accommodation coefficient (α), or the probability that a collision of a gas molecule with the aerosol surface leads to its incorporation into the aerosol.

Using the resistance model[24], the overall HO_2 uptake coefficient, γ_{HO2}, can be expressed as:

$$\frac{1}{\gamma_{HO2}} = \frac{1}{\gamma_{diffusion}} + \frac{1}{\alpha} + \frac{1}{\gamma_{reaction+partitioning}} \quad (1)$$

where the first term on the right hand side is resistance owing to gas-phase diffusion, and the third term is the resistance owing to the sum of reactive and partitioning processes within the aerosol. The mass accommodation coefficient can therefore be considered the upper limit value for γ when the gas-phase diffusion and aerosol-phase reactive/partitioning processes do not restrict the rate of gas uptake to the aerosol. Mozurkewich et al.[23] observed highly efficient uptake of HO_2 onto Cu(II)-doped aerosols with α_{HO2}>0.2 (the value depending on the Cu(II) molality), which has been confirmed in recent studies[25, 26].

HO_2 uptake has also been studied on dry salt films in low pressure flow tubes at a range of temperatures[27-29] with room temperature uptake coefficients for NaCl films in the range of γ_{HO2}=0.002-0.016 as shown in Table 1. The atmospheric relevance of these film studies is somewhat limited, however, due to (i) the gas diffusion limitations of

high uptake values, (ii) high HO_2 concentrations that can lead to second-order reactive processes occurring within the aerosol (see below) and (iii) differences in physical characteristics of film and aerosol surfaces[30]. Several more recent uptake studies have measured HO_2 uptake coefficients onto submicron salt aerosols in the presence and absence of Cu(II) ions[25, 31, 32, 33]. Thornton and Abbatt[32] measured HO_2 uptake onto aqueous $(NH_4)_2SO_4$ and H_2SO_4 aerosols with an aerosol flow tube and a Chemical Ionization Mass Spectrometer. In this study, the loss of HO_2 radicals onto buffered aqueous $(NH_4)_2SO_4$ aerosols at pH=5.1 was suggested to be second order with respect to HO_2 while reporting an uptake coefficient of γ_{HO2}~0.1 assuming first-order kinetics for comparative purposes. Furthermore, much slower uptake on H_2SO_4 aerosols (γ_{HO2}<0.01) was observed at room temperature. The kinetics observed in that study were consistent with known pH-dependent aqueous bulk HO_2 chemistry including the following aqueous reactions (R1)-(R3):

$$HO_2 \rightleftharpoons H^+ + O_2^- \quad \text{(R1)}$$

$$HO_2 + HO_2 \rightarrow H_2O_2 + O_2 \quad \text{(R2)}$$

$$HO_2 + O_2^- \xrightarrow{H_2O} H_2O_2 + O_2 + OH^- \quad \text{(R3)}$$

Because high HO_2 concentrations ($[HO_2]$~5×10^{10} molecule cm^{-3}) were used, very slow HO_2 uptake (γ_{HO2}<0.01) onto aqueous aerosols was predicted by extrapolation of the observed second-order kinetics to atmospheric HO_2 concentrations at room temperature and in the absence of transition metal ions.

In contrast, Taketani et al.[25, 33] measured much higher HO_2 uptake coefficients onto aqueous $(NH_4)_2SO_4$, NaCl and the water-soluble fraction of ambient aerosols at room temperature (γ_{HO2}=0.09-0.4) using an aerosol flow tube coupled to a HO_2 detection system. The method is based on chemical conversion to OH via the addition of NO followed by laser-induced fluorescence detection of OH at low pressure (the Fluorescence Assay by Gas-Expansion (FAGE) technique)[34, 35]. Using this method, Taketani et al.[25] were able to conduct HO_2 uptake measurements under atmospherically relevant HO_2 concentrations, i.e. $[HO_2]$~10^8 molecule cm^{-3}. Apart from the work of Thornton and Abbatt[32], most studies have observed first-order HO_2 loss kinetics. Furthermore, Taketani et al.[25] reported the first results to indicate a large enhancement

in HO_2 uptake onto aqueous salt aerosols compared to dry aerosols. There have been few studies of the products formed following uptake into the aerosol that may shed light on the reaction mechanism. In one study, H_2O_2 was observed[28] that is consistent with the reaction mechanism above (Reactions (R1)-(R3)). Recently, Mao et al.[36] proposed an alternative aqueous-phase mechanism that does not lead to the formation of H_2O_2, with implications for the production rate of HO_x in the atmosphere. However, this catalytic mechanism involving aerosol-phase transition metal redox cycling has not yet been confirmed by experimental work.

It is clear from Table 1 that there is a significant range in the HO_2 reactive uptake coefficients values reported for salt aerosols at room temperature. As a result, an accurate parametrization of the rate of HO_2 loss in models cannot be achieved with the limited laboratory experiments currently available. Therefore, to reduce the uncertainty in the uptake coefficient, new laboratory studies were conducted to investigate the kinetics of HO_2 radical uptake onto submicron salt aerosols at room temperature. HO_2 reactive uptake coefficients were measured using an aerosol flow tube coupled to the FAGE technique that allowed for measurements to be conducted under atmospherically relevant HO_2 concentrations ($[HO_2] = 10^8$ to 10^9 molecule cm^{-3}). In order to try to explain the discrepancies with previous measurements, experiments were performed whilst varying a wide range of parameters, including the relative humidity, HO_2 concentration and the reaction time.

2. Experimental

The aerosol flow tube system is shown schematically in Figure 1. All flows in most of the experiments were generated from compressed N_2 passed through a gas purification system (TSI 3074B) consisting of particle filters, dryer and carbon filter prior to use. For experiments conducted in air, cylinders of purified air (BOC, BTCA 178) were used. The major components of the experimental system will be described in detail below.

2.1. Aerosol generation and characterization

Polydisperse salt aerosols were produced from aqueous salt solutions using a commercial constant output atomizer (TSI 3076). The 1% w/v aqueous salt solutions contained either ammonium sulfate (Fisher Scientific, ≥99%), ammonium nitrate

(Sigma-Aldrich, ≥99.5%) or sodium chloride (Fisher Scientific, ≥99.9%) dissolved in 18.2 MΩ-cm water (ELGA PURELAB). All solutions used in these experiments underwent an analysis for trace metals content (in particular transition metal ions) using inductively coupled plasma mass spectrometry (ICP-MS). Based on these analyses, it was deemed necessary to prepare fresh solutions daily to avoid trace metal contamination. The mass accommodation of HO_2 (α_{HO2}) was measured using Cu(II)-doped ammonium sulfate aerosol produced from atomizer solutions of copper sulfate pentahydrate (Fisher Scientific, Laboratory Reagent Grade) in 0.02 M ammonium sulfate with a molar ratio of 1:20. A fraction of the aerosol flow from the atomizer was discarded using a needle valve. Dry NaCl and $(NH_4)_2SO_4$ aerosol particles were produced by passing the flow from the atomizer through a diffusion dryer (TSI 3062) to reduce the relative humidity (RH) to RH<15%, thereby inducing particle efflorescence (i.e. crystallization) that occurs in the range of RH~35-40% for these salts[37, 38]. The dry particles remained in the crystallized phase up to their deliquescence humidities, i.e. RH~75-80%[37, 38]. The dryer was bypassed for experiments with aqueous salt particles. Ammonium nitrate particles remained in the aqueous phase for all experiments in this work due to their inability to efflorescence down to RH=2%[38].

The aerosol flow was then passed through an aerosol neutralizer (Grimm 5522) positioned directly after the atomizer. The neutralizer imparts a known electrical charge distribution on the particles to facilitate an accurate particle sizing measurement and to reduce particle losses throughout the experimental system. An impactor with a 0.071mm nozzle (TSI 1035900) was used to remove large particles and to monitor the aerosol flow rate that was kept at ~1.0 lpm (standard litres per minute). At this flow rate, the impactor removes 50% or more of all particles above 685 nm (i.e. D50 cutoff = 685 nm). Aerosol particle concentrations were varied by changing the fraction of the aerosol flow that passes through a High-Efficiency Particulate Air (HEPA) filter while keeping the total aerosol flow rate constant. The humidity of the aerosol flow was adjusted by mixing it with a humidity-controlled N_2 flow in a conditioning glass flow tube (40 cm length, 3 cm I.D., residence time ~ 4 s). The humidified flow was produced by combining a dry N_2 flow and a second humidified N_2 flow controlled by two calibrated mass flow controllers (MKS 1179) with a combined flow rate of ~3 lpm. The

wet N_2 flow was humidified by passing a dry N_2 flow through a temperature-controlled water bubbler.

The aerosol size distribution and total aerosol number concentrations were measured with a Scanning Mobility Particle Sizing (SMPS) instrument from the flow exiting the aerosol flow tube, as shown in Figure 1. The SMPS consisted of a Differential Mobility Analyzer (DMA, TSI 3080, 3081) that scanned particle sizes based on their electrical mobility, while a condensation particle counter (TSI 3775) quantified particle number concentrations. Accurate particle number concentrations and size distributions can be calculated by the SMPS based in particle electrical mobilities only if the particle charge distribution is known. For this reason, the SMPS includes a neutralizer (TSI 3077), which applies a Boltzmann charge distribution to the aerosol particles before entering the DMA to be separated and quantified based on their electrical mobility. The efficiency of the TSI neutralizer to neutralize particles exiting the reaction flow tube with the expected charge distribution was determined by comparing particle number concentration measurements of the SMPS with those taken by a second CPC (TSI 3775). Both SMPS and CPC sampled the same flow of aqueous NaCl aerosol particles while the aerosol concentration was varied from 0 to ~10^6 cm^{-3}. The particle concentration comparisons using one or two neutralizers is shown in Figure 2. All measurements were taken with the flow to the SMPS passing through the TSI neutralizer. One set of measurements was taken with a second Grimm neutralizer placed just after the aerosol flow exits the atomizer. The SMPS overpredicted particle number concentrations by up to ~35% using only one neutralizer compared to two neutralizers for high particle concentrations of $N>6\times10^5$ cm^{-3}.

The SMPS scanned over the mobility diameter range of 15–700 nm, and from the size distributions the total aerosol surface area was calculated assuming particles were spherical. Typical mean surface-weighted diameters were in the range of D_s=100-200 nm and geometric standard deviation of the size distributions was in the range σ_g = 1.5-1.8. Aerosol surface area concentrations during the kinetic experiments were in the range of 0 to 1×10^{-3} cm^2 cm^{-3} and particle number concentrations ranged from 0 to 2×10^6 cm^{-3}. Because the particle size of aqueous aerosols is sensitive to humidity, the RH of the recirculating sheath flow exiting the DMA was monitored with a RH probe

(Rotronic HygroClip2, accuracy 0.8% RH) to confirm that aerosols were being measured under the same humidity conditions as were present in the flow tube.

2.2. Generation and delivery of HO_2 radicals

HO_2 radicals were produced from the 184.9 nm photolysis of H_2O vapour using a mercury penray lamp (L.O.T.-Oriel 6035) housed inside the stainless steel movable injector (110 cm length, 1.9 cm O.D., 1.6 cm I.D.). Water vapour was introduced into the injector by humidifying a flow of nitrogen using a temperature-controlled bubbler followed by dilution using a flow of dry N_2. The photolysis of water vapour in the injector flow resulted in production of H atoms that subsequently reacted with trace O_2 in the N_2 flow (normally specified as 20-30 ppm from the N_2 generator) to generate HO_2 radicals as follows:

$$H_2O + h\nu\ (\lambda=185\ nm) \rightarrow OH + H \quad \text{(R4)}$$

$$H + O_2 + M \rightarrow HO_2 + M \quad \text{(R5)}$$

Assuming a 30 ppm mixing ratio of O_2, the lifetime of the H atom by reaction with O_2 is ~ 17 μs, leading to rapid and quantitative conversion to HO_2 in the injector. Indeed, when synthetic air was used rather than N_2 in some experiments, a similar HO_2 signal was measured by FAGE. The dry and wet N_2 flows making up the injector flow were controlled by calibrated mass flow controllers (MKS 1179) giving a combined flow rate of 1.3 lpm. Air was not used for the majority of the experiments in order to prevent the production of O_3 (>1 ppm observed in the main flow-tube when using air) upon photolysis of O_2 at 184.9 nm in the injector by the mercury lamp, which could lead to significant gas-phase loss of HO_2 radicals or aerosol modification. However, some experiments were performed in air (BOC, BTCA) in order to show that uptake coefficients measured in air were the same as performed in N_2 (see Section 3.6).

Downstream of the HO_2 production region, the injector flow carrying HO_2 radicals was introduced into the reaction flow tube through the tip of the injector. The mercury lamp was located in a part of the injector that was kept outside the reaction flow tube at all times, to reduce any heating effects. A Teflon tube insert (1.5 cm O.D., 0.8 cm I.D.) was placed inside the injector to minimize any HO_2 radical losses to the injector wall. Moreover, fans placed externally to the injector were used to dissipate any

heat from the lamp. Although OH radicals were produced along with HO_2 radicals, they were not detected in the aerosol flow tube, even close to the injector tip, indicating they were reactively lost within the injector. This is explained in more detail in Section 2.5.

2.3. Detection of HO_2 radicals

HO_2 radicals were detected using the Fluorescence Assay by Gas Expansion (FAGE) technique, which has been successfully utilized in field studies for the *in situ* measurement of tropospheric OH and HO_2[14, 34, 35]. HO_2 radicals were measured using the addition of NO inside the detection cell to convert HO_2 to OH with subsequent on-resonant LIF detection of OH radicals via excitation of the $A^2\Sigma^+$ $(v'=0)\leftarrow X^2\Pi_i$ $(v''=0)$ $Q_1(2)$ transition at ~308 nm. The FAGE technique has been described in detail previously[15], so only a concise description is given here focusing on modifications made to interface the FAGE detection cell to the aerosol flow tube.

As shown in Figure 1, the FAGE cell (22 cm ID) sampled through a 0.7 mm diameter pinhole mounted on a flat plate placed on the central axis and 4.3 cm from the end of the aerosol flow tube. The fluorescence cell was one previously used for field measurements of OH and HO_2 radicals that housed the fluorescence collection optics within a central rail. A roots blower/rotary pump combination (Edwards EH1200, E1M80) evacuated the FAGE cell, which was held at a constant pressure of 0.6-0.7 Torr monitored by capacitance manometer (Tylan General, CDL11). The volumetric flow through the sampling pinhole was ~3.4 lpm. These operating conditions of the cell (pressure, flow, pinhole diameter) were optimized for maximum HO_2 sensitivity. The OH fluorescence lifetime is lengthened via expansion to low pressures, so that electronic gating of the detector discriminates against the collection of background signal originating from scattered light during the laser pulse. Wavelength-tunable 308 nm radiation was generated by a frequency-doubled dye laser (Sirah Laser-und Plasmathechnik, GmbH) pumped by 532 nm radiation from an Nd-YAG laser (JDSU Q201-HD Q-series) running at 5 kHz pulse repetition frequency. The UV light exiting the laser passed through a beamsplitter (Melles Griot), with 10% directed towards an OH reference LIF cell. In the OH reference cell, high concentrations of OH radicals were produced via the thermal decomposition of H_2O by passing a humidified air flow over a heated filament nichrome wire, that had 5.3 amps applied through it[13]. The OH

reference cell was kept at a constant pressure of 2 Torr and the partial pressure of the water vapour was 0.05 Torr. The OH reference cell was equipped with fluorescence collection optics and a photomultiplier (Perkin Elmer 993P). The OH LIF signal measured as a function of laser wavelength was used to locate the peak of the OH $Q_1(2)$ rotational line. This "online" wavelength was held constant for the duration of the experiment.

The remainder of the 308 nm light was delivered to the FAGE cell via a fibre launcher (Oz Optics), 5 m of optical fibre cable (Oz Optics), a fibre collimator (Oz Optics), and a sidearm containing optical baffles to reduce scattered light. The 308 nm laser power exiting the fibre was typically 10-20 mW. The laser radiation and the gas flow were perpendicular to one another. The fluorescence from OH (converted from HO_2) was imaged perpendicularly to both the laser light and gas flow using fast optics and passed through a 308 nm bandpass filter (Barr Associates, 308 nm., FWHM= 8 nm) and focused onto the photocathode of a channel photomultiplier (CPM) (Perkin Elmer, C-943P) held at -2900 V). A home-built gating system (a modified form of the one described in Creasey et al.[39]) was used to switch the CPM off during the laser pulse to avoid optical damage. The CPM then was switched on again 205 ns after the beginning of each laser pulse. After passing through a discriminator held at -4.7 mV, the signal from the CPM was processed by a gated photon counting card (Becker and Hickl GmbH, PMS-400). Starting 150 ns after the laser pulse, photons were counted for 1 μs (the "A" gate signal, A_{sig}). The total signal includes OH LIF photons, scattered light at ~308 nm (either from the laser or room light entering the cell through the sampling pinhole) and CPM dark counts. A further 10 μs later, the background signal was collected for 20 μs (the "B" gate signal, B_{sig}). The signal due to the sum of OH LIF and laser scattered light was background subtracted using A_{sig}-(B_{sig}/20). The laser power was monitored after exiting the cell through a second baffled sidearm by a photodiode (New Focus, 2032), and was used to normalize the sum of the total signal. The laser power typically varied less than 2% over the time required to record a decay of HO_2 in the aerosol flow tube.

Nitric oxide (BOC, 99.5%) used to convert HO_2 to OH in the FAGE cell was delivered into the cell through four 1/8" OD stainless steel injection ports arranged symmetrically around the gas flow sampled from the flow tube and ~5 cm downstream

of the sampling pinhole. The NO flow (50 sccm) was controlled by a calibrated mass flow controller (Brooks 5850S) and converted ~70% of the HO_2 to OH. Absolute HO_2 concentrations were determined from the OH LIF signals using a turbulent-flow calibration system to generate HO_2 and described in detail elsewhere[40]. Equal concentrations of OH and HO_2 radicals were produced via 184.9 nm photolysis of H_2O vapour by passing 40 slpm of humidified synthetic air flow through a rectangular flow tube with a 1.61 cm^2 cross sectional area. The humidified flow was illuminated by a mercury penray lamp positioned behind a Suprasil window and in a housing purged with a dry N_2 flow and heated to ~40°C to maintain a constant lamp output. The product of the photon flux and the residence time of the 184.9 nm radiation within the calibration flow tube was obtained using an N_2O actinometer with detection of NO[41]. The air flow from the calibrator was directed at the FAGE cell sampling pinhole and used to obtain the LIF signal for a known HO_2 concentration, from which the HO_2 detection limit of $[HO_2]_{min}=1\times10^7$ molecule cm^{-3} was obtained for 3 second signal averaging and a signal to noise ratio of unity. Typical initial HO_2 concentrations exiting the injector during the heterogeneous uptake experiments were in the range of 1.5×10^8 to 1.5×10^9 molecule cm^{-3}.

One potential contribution to the observed LIF signal is Mie scattering of the laser radiation from the aerosols sampled into the FAGE cell. However, the background signals obtained either while the laser wavelength was tuned offline or online with the Hg lamp off, did not change with aerosol concentration in the flow tube. This clearly indicates that Mie scattering did not contribute towards the observed LIF signals.

2.4. Aerosol flow tube

The aerosol flow tube was a horizontally-oriented glass tube whose inner walls were coated with halocarbon wax (Halocarbon Wax Corporation, 600) to minimize HO_2 loss to the flow tube wall. Two different coated flow tubes of similar dimensions (100 cm and 107 cm length, both 5.9 cm ID) were used over the duration of this work. There was no observable difference in results using the different flow tubes. The aerosol flow tube was kept at ambient pressure and temperature (T~19° C), where the latter was monitored by thermocouples inside the flow tube. The downstream end of the flow tube was connected to the FAGE cell by a compression fitting with a Viton O-ring seal. The

aerosol flow exiting the conditioning flow tube (see Figure 1) was introduced to the upstream end of the flow tube through two inlet ports. Aerosol particle losses along the entire length of the flow tube were measured periodically and were found to be negligible, i.e. within the error of CPC measurement (<10%). In addition, the aerosol size distribution did not change significantly along the length of the flow tube.

The movable injector was situated along the central axis of the flow tube. The injector flow containing HO_2 was introduced into the main reaction flow tube from a Teflon injector tip containing 20 holes of 1 mm diameter drilled equally around the circumference of its side and 0.5 cm from the end of the injector tip. Because of this arrangement, the injector flow initially entered the reaction flow tube perpendicular to the flow containing the aerosols to facilitate mixing of HO_2 with the main flow. The volumetric flow rates of the aerosol and the injector flows were measured before entering the reaction flow tube with a flow meter (TSI 4140). The sum of these two flow rates was in the range of 5.2-5.7 lpm giving a Reynolds number of ~130. Therefore, the flow should be in the laminar regime with a corresponding bulk linear flow velocity between 3.2 to 3.5 cm s^{-1}. The mixing time (t_D) due to diffusion of one gas into another under laminar conditions is given by $r^2/5D_g$, where D_g is the diffusion constant and r is the flow tube radius[42]. A mixing time of t_D ~7 s was calculated using the HO_2 diffusion constant in O_2 (and assumed to be the same for N_2) of $D_{g,HO2}$ = 0.25 cm^2 s^{-1} [23], which corresponds to a mixing length of 24 cm under typical flow conditions in these experiments. As the HO_2 flow was introduced into the reaction flow tube perpendicularly to the main flow, some degree of local turbulence is introduced. Therefore, the rate of mixing should be enhanced and the actual mixing time is shorter than the theoretical value previously calculated assuming laminar flow.

Complete mixing of the injected flow into the main flow containing aerosol particles was confirmed by two different methods. The first method involved measuring ozone concentrations at a fixed point in the centre of the aerosol reaction flow tube as a function of the distance from the tip of the injector. O_3 was generated inside the injector from the following reactions by introducing synthetic air into the injector:

$$O_2 + h\nu\ (184.9\ nm) \rightarrow 2\ O(^3P) \quad \text{(R6)}$$

$$O(^3P) + O_2 + M \rightarrow O_3 + M \quad \text{(R7)}$$

An O_3 analyzer (ThermoElectron 49 C, detection limit = 1 ppb) sampled the flow in the centre of the aerosol flow tube through a 1/4" OD tube pointing into the flow. A typical axial ozone profile is shown in Figure 3. The ozone concentration stabilizes to a constant value (with a standard deviation of 4%) after ~30 cm downstream of the injector. Therefore, all experiments involving moving the injector to measure HO_2 uptake coefficients were conducted for injector tip to FAGE sampling distances of greater than 30 cm (typically 40 to 70 cm was used). Injector positions will be reported in the following text as the distance from the end of the flow tube connected to the main face of the FAGE cell (defined as 0 cm). The minimum distance that could be achieved in practice was 4.3 cm owing to the physical dimensions of the assembly upon which the sampling pinhole was mounted (see Figure 1).

The second method used to probe the extent of mixing involved translating the injector away from the FAGE cell and measuring the HO_2 signal. The extent of mixing was determined by measuring the variation of the HO_2 signal as the injector was moved towards and away from the FAGE cell, taking particular note of the signal variation very close to the injector tip. As the HO_2 flow was injected perpendicularly to the aerosol flow, it was expected that it would take a certain amount of time for the HO_2 to mix/diffuse into the centre of the flow tube from where the FAGE cell was sampling. As shown in Figure 4, initially the signal increases with distance as the HO_2 mixes back to the centre of the flow and is sampled by the FAGE inlet. Thus, the signal increase due to mixing outweighs the reduction in HO_2 with distance through loss to the wall and uptake on aerosols in that short period. Once HO_2 is mixed, the signal then decreases owing to wall loss and uptake onto the surface of aerosols. Although there is initially some structure to the decay owing to residual mixing, HO_2 would appear to be mixed into the main flow by ~15 cm downstream of the injector. It is stressed again that uptake measurements of HO_2 do not begin until 40 cm downstream from the injector for normal moving injector experiments and 20 cm for fixed injector experiments to ensure well mixed flows.

2.5. Experimental procedure and data analysis

HO_2 uptake experiments were conducted by measuring the reduction in HO_2 signal using the FAGE detector while varying the position of the movable injector along

the reaction flow tube, thereby changing the reaction time between HO_2 radicals and aerosol particles. The FAGE cell sampled ~3.4 lpm of the total flow. As shown in Figure 1, the remainder of the flow exited through a sidearm of the reaction flow tube near the end connected to the FAGE cell, of which 0.3 splm was sampled by the SMPS. The RH of the remainder flow was also monitored with a probe (Rotronic Hygroclip2). Prior to experiments, all flows were allowed to equilibrate for at least 30 minutes or until the RH readings for both the DMA sheath flow and the remainder flow from the reaction flow tube were stable to within 1% of the desired RH.

Prior to the measurement of a HO_2 decay, the background signals from the following sets of experimental conditions at the initial injector position at 30 cm were measured: (A) injector lamp turned off, NO flow to the FAGE cell turned off; (B) injector lamp turned on (HO_2 production) and NO flow turned off; (C) injector lamp turned off, NO flow turned on. The background signals in experiments (A) and (B) were in agreement to within 10%, demonstrating that any OH generated in the injector does not survive to the FAGE sampling region above the detection limit of the instrument. Experiment (C) generated a slightly larger background (~15%) than (A) or (B), which remained constant with injector position. This background signal (C) was subtracted from the HO_2 signal for all experiments.

Assuming that the rate determining step is first order in HO_2, the time evolution of the HO_2 concentration can be written as:

$$ln\,[HO_2]_t = ln\,[HO_2]_0 - k_{obs}t \qquad (2)$$

where $[HO_2]_t$ and $[HO_2]_0$ are the HO_2 concentrations at reaction time t and t=0, respectively, and k_{obs} is the observed pseudo first-order rate constant for loss of HO_2. In these experiments, we define $[HO_2]_0$ as the HO_2 concentration at the initial injector position of 40 cm (i.e. a distance of 35.7 cm from the FAGE inlet to the injector tip). As the LIF signals from HO_2 are directly proportional to the HO_2 concentrations, the LIF signals were used instead of concentrations in Equation (2).

Figure 5 shows a typical decay with the natural log of the background subtracted HO_2 signal plotted as a function of the injector position from 40 to 70 cm both in the absence and presence of aerosols. The position of the injector during the experiment

was mechanically controlled by a linear drive (BSL Engineering 15 KR4610A) to an accuracy of 0.25 mm, controlled from the computer. During an experiment, the injector was first stepped backwards from 30 to 75 cm in 1 cm increments, and then stepped forward in a similar manner back to 30 cm. The HO_2 signal was averaged over 3 s (average of three 1 s measurement points, each corresponding to 5000 laser shots) at each injector position with a 3 s delay time between each step to allow any mechanical vibrations to subside. For data analysis, the measurements taken between 40 and 70 cm were analyzed where the flow was fully mixed (see above) and in the laminar regime according to the calculated Reynolds number. The decrease in ln(HO_2 signal) with increasing injector position was observed to be linear for all experiments in the presence or absence of aerosols, consistent with Equation (2) and with first-order uptake kinetics in HO_2. Non-exponential decays were observed at smaller injector positions, particularly below 30 cm, as shown in Figure 4. This will be discussed further in Section 3.4 below. The bulk flow velocity, calculated using the volumetric flow rate and the cross-sectional area of the flow reactor, was used to convert injector position to relative reaction times. The observed pseudo first-order rate constants for HO_2 uptake (k_{obs}) were calculated from the error-weighted linear least squares fit of Equation (2) to the ln(HO_2 signal) with injector position as shown in Figure 5.

The rate constants calculated from the linear fits to the data obtained by moving the injector backwards or forwards were consistent with each other within the 1σ statistical error of the fits. Therefore, the data obtained from the injector moving forwards and backwards were averaged and will not be distinguished in the following text. The k_{obs} values were measured in the absence of aerosols (referred to as wall loss experiments) several times throughout each experiment. The k_{obs} values were determined in the presence of aerosols for at least five different aerosol concentrations. As noted previously, the aerosol concentrations were adjusted by varying the fraction of the aerosol flow passing through a HEPA filter while keeping all flow rates and the RH constant. The entire aerosol flow was passed through the filter for the wall loss experiments. The k_{obs} values obtained from the wall loss experiments were used to correct the k_{obs} values taken in the presence of aerosols for gas-phase diffusion under non-plug flow conditions using the iterative procedures as outlined by Brown (1978). The Brown correction[43] increased the first-order rate constants (k_{obs}) by ~ 10 to 40%

depending on the measured wall loss. An example of the Brown corrected rate constants, k', as a function of total aerosol surface area, S_a, is shown in Figure 6a and 6b for aqueous Cu(II)-doped $(NH_4)_2SO_4$ and $(NH_4)_2SO_4$ aerosols along with linear least squares fits to the data of the following function:

$$k' = \frac{\gamma_{obs} v_{HO2} S_a}{4} \quad (3)$$

where ν_{HO2} is the mean molecular velocity of HO_2 (cm s^{-1}) and S_a is the total aerosol surface area per unit volume (cm^2 cm^{-3}).

As discussed above, Equation (1) indicates that gas diffusion to the aerosol can limit γ_{obs}, particularly for uptake onto large aerosol particles or for large uptake coefficient values. Therefore, the experimentally determined γ_{obs} values need to be corrected for gas diffusion using Equation (4) as suggested by Fuchs and Sutugin[44]. The values of γ_{HO2} reported here include 2σ random errors (95% confidence limits) from fits of Equation (3) to the data and systematic errors from the accuracy of the mass flow controllers (3%) and the aerosol concentrations measured using the CPC (10%).

$$\gamma_{HO2} = \frac{\gamma_{obs}}{\left(1 - \gamma_{obs}\lambda(r)\right)} \quad (4)$$

where $\lambda(r)$ is a function of the Knudsen number (K_n=3 D_g /ν_{HO2} r) and given by:

$$\lambda(r) = \frac{0.75 + 0.283K_n}{K_n(1 + K_n)} \quad (5)$$

For the range of particle radii, r, used in this work, the diffusion corrections to γ_{HO2} and α_{HO2} were <1% and 4%, respectively.

3. Results and Discussion

Table 2 summarizes the HO_2 reactive uptake coefficients onto aqueous and dry salt aerosol particles measured for a range of relative humidities. In cases where the losses of HO_2 with and without the presence of aerosols were indistinguishable, an

upper limit value is stated. Upper limits of γ_{HO2} values were calculated from 2σ of the mean wall loss determined for each experiment.

3.1. Uptake onto dry salt aerosols

HO_2 uptake was measured onto dry $(NH_4)_2SO_4$ and NaCl particles at a low (RH~30%) and medium (RH~50%) relative humidities (Table 2). The particle phase was confirmed by reducing the RH in the reaction flow tube to below the efflorescence RH, i.e. RH<35%, and observing no change in the distribution of aerosol particle diameters. Typical size distributions are shown in Figure 7a for dry $(NH_4)_2SO_4$ particles at an experimental humidity of RH 52% and for the dried aerosol flow (RH=13%). The HO_2 uptake values for all experiments with dry aerosols were below our limit of detection for these experiments of $\gamma<0.002$ and $\gamma<0.004$ for low and medium RH values, respectively.

Literature values for HO_2 uptake onto dry NaCl films and dry aerosol particles span an order of magnitude in the range γ_{HO2}=0.0018-0.02, as shown in Table 1. For HO_2 uptake onto dry $(NH_4)_2SO_4$, the reported literature values ranged from γ_{HO2}=0.011 for experiments with a solid film[27] to γ_{HO2}= 0.04-0.05 for dry particles[25]. The HO_2 uptake coefficients onto dry salts observed in this work are consistent with the low end of the reported values[28], but most literature values are significantly higher, i.e. γ_{HO2}=0.01-0.05. The concentration of water vapour (obtained from the RH) did not have an observable effect on γ_{HO2} values apart from increasing the rate of HO_2 loss to walls, and thus increasing the upper limits for γ_{HO2} values. Taketani et al.[25] found a significant increase in γ_{HO2} values for NaCl particles from <0.01 to 0.02 ($\pm$0.01) for RH = 20 and 45%, respectively. However, no significant change in uptake onto dry $(NH_4)_2SO_4$ particles was observed for the same increase in RH. In contrast, Remorov et al.[29] observed a reduction in the HO_2 uptake coefficient onto dry NaCl films with the addition of water vapour. The explanation for the large discrepancies between these studies is unclear, but experimental conditions such as pressure, humidity, number of available surface sites per surface area and deactivation of these sites may all play a role.

3.2. Uptake onto Cu(II)-doped aqueous aerosols

The mass accommodation of HO_2 to aqueous aerosols was determined by measuring the HO_2 loss onto aqueous $(NH_4)_2SO_4$ particles doped with Cu(II) ions. HO_2 radicals are rapidly and irreversibly scavenged by Cu^{2+} ions in the aqueous phase via the following catalytic reactions (R8)-(R11):

$$HO_{2(aq)} + Cu^{2+}_{(aq)} \rightarrow O_{2(aq)} + Cu^{+}_{(aq)} + H^{+}_{(aq)} \quad \text{(R8)}$$

$$O_2^{-}{}_{(aq)} + Cu^{2+}_{(aq)} \rightarrow O_{2(aq)} + Cu^{+}_{(aq)} \quad \text{(R9)}$$

$$HO_{2(aq)} + Cu^{+}_{(aq)} + H_2O_{(l)} \rightarrow H_2O_{2(aq)} + Cu^{2+}_{(aq)} + OH^{-}_{(aq)} \quad \text{(R10)}$$

$$O_2^{-}{}_{(aq)} + Cu^{+}_{(aq)} + 2H_2O \rightarrow H_2O_{2(aq)} + Cu^{2+}_{(aq)} + 2OH^{-}_{(aq)} \quad \text{(R11)}$$

If there are sufficient Cu(II) concentrations in the aerosol to drive this chemistry, the overall rate of HO_2 uptake to the aerosol is controlled by mass accommodation (α) onto the aerosol via transport processes rather than by irreversible reactions or solubility in the aerosol phase (i.e. the third term in Equation (1)). Mozurkewich et al.[23] found that HO_2 was most efficiently scavenged in aqueous NH_4HSO_4 and $LiNO_3$ aerosols for Cu(II) aerosol concentrations >0.05 molal. In this work, the estimated Cu(II) aerosol concentration was in the range 0.5-0.7 molal. Therefore, it is expected that $\gamma_{HO2} \approx \alpha_{HO2}$.

HO_2 uptake coefficients onto Cu(II) doped $(NH_4)_2SO_4$ aerosol particles were measured in the humidity range RH=53-65% in the range of α_{HO2}=0.26–0.64 and with a mean value of α_{HO2}=0.4±0.3. These α_{HO2} values are generally consistent with literature values for α_{HO2} onto Cu(II) doped aqueous salt aerosols, indicating that α_{HO2} >0.2. Taketani et al.[25] and Thornton and Abbatt[32] have both measured α_{HO2}~0.5, which fall within the measured range of values in this work. It should be noted that the reported error in our mean value reflects the large spread of values measured, which was much greater than the propagation of the random experimental errors for individual experiments. The relative standard deviation in individual mass accommodation measurements was 11% or less. The effect of HO_2 concentration and reaction time on the mass accommodation coefficient was significant and may partly explain the wide range in α_{HO2} values observed here. In general, the measured α_{HO2} values decreased with higher HO_2 concentrations and with reaction time. This will be discussed further in Sections 3.4 and 3.5.

3.3. Uptake onto aqueous salt aerosols without Cu(II) doping

As shown in Table 2, the measured γ_{HO2} values for aqueous $(NH_4)_2SO_4$, NaCl and NH_4NO_3 aerosols over a range of RH spanned from γ_{HO2}=0.003-0.016. The particle phase was also confirmed in an analogous manner as with the dry particle experiments discussed earlier. A reduction in the mean particle diameter was observed upon drying the aerosol flow to below the efflorescence RH of $(NH_4)_2SO_4$ particles (i.e. <35%) as shown in Figure 7b, indicating that aerosols were in the aqueous phase. In contrast to HO_2 uptake onto dry salt aerosols, the uptake onto aqueous salt aerosols was measurable for most experiments. These results indicate that the presence of condensed-phase water significantly enhances the irreversible loss of HO_2 within the aerosols. Few studies have measured HO_2 uptake onto both aqueous and dry salt aerosol particles without Cu doping. Although Taketani et al.[25] measured much higher uptake coefficients for aqueous $(NH_4)_2SO_4$ and NaCl particles (γ_{HO2}=0.09-0.19), they also reported enhanced HO_2 uptake onto aqueous aerosols compared to dry aerosols.

The effect of relative humidity was investigated by measuring HO_2 uptake onto aqueous NH_4NO_3 aerosols over a wide range of relative humidities. As noted previously, NH_4NO_3 particles remain in the supersaturated aqueous phase down to very low humidites (RH>2%). Experiments were conducted for relative humidities between approximately 30 and 70% in this work. This RH range corresponds to an aerosol mass fraction of condensed-phase water ranging from 10 to 41% as calculated from the Aerosol Inorganics Model[45]. The measured uptake coefficients showed no observable trend with RH within the range studied, as shown in Figure 8. It should be noted that in Table 2, the mean γ_{HO2} value of these individual experiments performed at different values of RH are given for aqueous NH_4NO_3 aerosols. The uptake experiments with NaCl and $(NH_4)_2SO_4$ aerosols were more variable than for NH_4NO_3 aerosols especially for higher relative humidities, but showed no clear dependence on RH within errors. Taketani et al.[25] observed a positive trend of γ_{HO2} values with RH for aqueous $(NH_4)_2SO_4$ aerosols, but not for uptake onto aqueous NaCl aerosols.

3.4. Time-dependent uptake kinetics

As noted above, reactive uptake coefficients were determined in the moving injector experiments for reaction times between 10–20 s after injection, i.e. for distances between 40 and 70 cm from the injector tip. The moving injector experiments revealed that HO_2 decay plots for uptake onto aqueous aerosols for reaction times <10 s, i.e. for injector positions <40 cm, were nonlinear and had larger gradients compared with reaction times of >10 s. The region with reaction times <10 s corresponds to reaction times where other studies (e.g. Taketani et al.[25]) have observed much higher uptake coefficients for aqueous salt aerosols with reaction times of ~5-11 s using a similar experimental setup and faster flow rates. Therefore, for comparative purposes the observed time-dependent HO_2 uptake was investigated further by performing fixed injector experiments instead of moving injector experiments that were described previously. Fixed injector experiments were conducted by holding the injector at a fixed position along the flow tube, and the reduction of the HO_2 signal was observed whilst the aerosol surface concentrations were increased. For a fixed reaction time, t, the HO_2 loss kinetics in the absence of aerosols can be written as:

$$\frac{\ln[HO_2]_{t,aerosol=0} - \ln[HO_2]_0}{t} = -k_{wall} \quad (6)$$

where $[HO_2]_0$ is the concentration at t=0 (at the injector tip). In the presence of aerosols, the kinetics can be described as:

$$\frac{\ln[HO_2]_{t,aerosol} - \ln[HO_2]_0}{t} = -k_{wall+aerosols} \quad (7)$$

Subtracting Equation (6) from Equation (7), which is analogous to subtracting the wall loss in the absence of aerosol for the moving injector experiment, gives:

$$\frac{\ln[HO_2]_{t,aerosol} - \ln[HO_2]_{t,aerosol=0}}{t} = k_{wall} - k_{wall+aerosols} = -k_{obs} \quad (8)$$

It is not necessary to define or to know the concentration of HO_2 at the injector tip. Figure 9(a) shows the dependence of ln(HO_2 signal) as a function of aerosol surface area for a range of injector positions from 20 to 70 cm for aqueous $(NH_4)_2SO_4$ aerosols at RH=65%. The left hand term in Equation (8) was then used to calculate k_{obs}. The k_{obs} values were converted into k' using the Brown correction and were then plotted versus aerosol surface area for each injector position, as shown in Figure 9(b). The γ_{obs} values were then obtained using Equation (3), and were corrected for gas-phase diffusion with

Equations (4) and (5) to determine γ_{HO2} values. It is important to note that the values of γ_{HO2} are not instantaneous values at each exposure time. Rather, they represent the cumulative uptake averaged over a given reaction time that HO_2 has been exposed to the aerosol from the injector tip to the FAGE sampling pinhole. Fixed injector experiments allowed the cumulative uptake of HO_2 on aerosols to be measured for different reaction times. In general, they yielded k' values with a smaller experimental error compared to those obtained in the moving injector experiments.

In Figure 9(b), it can be seen that the gradient, and hence γ_{HO2}, is a function of the reaction time with the values decreasing at longer times. Figure 10 shows the dependence of γ_{HO2} on reaction time (in the range 4-21 s corresponding to injector positions 20-70 cm) for aqueous $(NH_4)_2SO_4$ aerosols at RH=54-75%, aqueous NH_4NO_3 aerosols at RH=20% and aqueous NaCl aerosols at RH=60-65%. For comparison, the γ_{HO2} values obtained from the moving injector experiments are also shown as solid lines in Figure 10. In the moving injector experiments, the HO_2 decays were obtained between injector positions of 40-70 cm, corresponding to t~10- 20 seconds. Figure 10 shows that γ_{HO2} values obtained from the fixed injector experiments decreased over time and tended to a single value at longer times. These time-integrated γ_{HO2} values are higher than those determined from moving injector experiments. This is not surprising, as the fixed injector values include HO_2 uptake onto fresh aerosols and the HO_2 dilution and mixing region. If the heterogeneous kinetic processes that control HO_2 uptake remained constant over the entire reaction time period (0 to ~20 s), the γ_{HO2} values should be time independent. Further, γ_{HO2} values should be the same as the values reported in Table 1 from the moving injector experiments as indicated by the solid lines in Figure 10. However, it is apparent that HO_2 uptake is faster at shorter reaction times (<10 s) on aqueous aerosol compared to the timescales for the moving injector experiments (~10-20 s). This behavior is also shown in Figure 9(a) and (b), where the gradients change quickly at early times, then tend to constant values at later times.

Pseudo first-order kinetics were observed during the moving injector experiments between 40 and 70 cm, as shown in Figure 5. This indicates that quasi steady-state conditions in the processes controlling the rate of HO_2 uptake appear to have been reached. The decreasing uptake values with increasing reaction times from the fixed injector experiments were observed because the uptake at short reaction times

(<10 s) was initially high, followed by slower uptake at longer times settling to a constant value. HO_2 uptake was observed to be below the detection limit (γ_{HO2}<0.004) during a fixed injector experiment at an injector position of 40 cm (reaction time = 10.6 s) for dry $(NH_4)_2SO_4$ aerosol at RH=54%, which is consistent with the moving injector experiments. Hence, it was not possible to determine whether there was also a time-dependent uptake for dry aerosol particles.

Loukhovitskaya et al.[28] also report smaller HO_2 uptake coefficients with increasing HO_2 exposure time onto dry NaCl films. However, this observation was attributed to deactivation of the salt surface by nonreactive adsorption of HF to reactive surface sites, a byproduct formed from their HO_2 production methods. They did not perform experiments with aqueous salt surfaces. Therefore, it is unclear whether deactivation of aqueous surfaces over time will impact the value of the HO_2 uptake coefficient. The experimental system used in this work does not contain HF. Therefore, it is unlikely that deactivation of the aerosol surface with time as was observed by Loukhovitskaya et al.[28] can be used to explain the time dependence for HO_2 uptake onto salts observed in this work.

There are several possible explanations for the time dependence of the measured HO_2 uptake coefficients. There may be a trace contaminant in the aerosol phase that is highly reactive towards HO_2 and reacts away over the shorter timescales. The most likely reactive contaminants are transition metals, such as Cu and Fe ions, which may be present in the salts in trace amounts. Several of the salt solutions used in the atomizer were tested for Cu and Fe ions after use with ICP-MS. Both Cu and Fe concentrations in the salt solutions were found to be less than 1.8 μM. The HO_2 uptake coefficients varied significantly as a function of the transition metals ions concentration. These studies will be described in a forthcoming paper. However, there was no enhanced HO_2 uptake onto aerosols produced from atomizer solutions containing less than 1.8 μM Cu or Fe. Consequently, copper and iron contamination cannot explain the observed time dependence of HO_2 uptake.

Another possible explanation is that the aerosol surface coverage of HO_2 is initially time dependent before the aerosol surface becomes saturated. After the aerosol surface reaches saturation equilibrium with gas-phase HO_2, HO_2 uptake is then controlled by partitioning within the aqueous phase or reaction. Ammann and Pöschl[46]

conducted modeling simulations of nonreactive heterogeneous uptake kinetics of a gas onto solid and liquid aerosols under various conditions that may help to interpret our findings. In general, the modeling predicts that the gas uptake coefficient to a liquid aerosol will be equal to the mass accommodation coefficient until the gas concentration in the aerosol phase reaches its saturation equilibrium concentration. Once this point is reached, γ then drops quickly to zero.

The time dependent HO_2 uptake kinetics was explored further by conducting a fixed uptake experiment for Cu(II)-doped $(NH_4)_2SO_4$ aerosol. HO_2. As shown in Figure 11, mass accommodation values decreased with increasing reaction times similar to the observed trends in the HO_2 uptake values. Because the observed mass accommodation values were much higher than the reactive uptake values, mass accommodation is likely not the limiting factor to overall uptake. Therefore, the observed time dependence of HO_2 uptake cannot directly be attributed to changes in the mass accommodation values with time. The observed time dependences in both overall HO_2 uptake and mass accommodation would be consistent with surface saturation effects as discussed above. However, modeling of the uptake kinetics would be necessary to conclusively determine the kinetic mechanisms responsible for these observations. The KM-SUB (Kinetic multi-layer model of aerosol surface and bulk chemistry) model[47] is currently being adapted to enable the uptake of reactive radicals onto an aerosol surface to be studied. We plan to use the model to further explore the observed time dependences in our data.

3.5. Dependence of the uptake coefficients upon HO_2 concentration

The dependence of γ_{HO2} on the HO_2 concentration was examined by conducting both moving and fixed injector experiments. The FAGE detection system was calibrated for HO_2 concentration, and so the signal at any point in the flow tube can be converted to an absolute concentration. Initial HO_2 concentrations were estimated by using the calibrated HO_2 signal at 40 cm injector position in the absence of aerosols and the value of k_{obs} in the absence of aerosol to extrapolate back to t=0. Although the calibration enables a precise value of [HO_2] at 40 cm, the extrapolation does not reflect the actual concentration exiting the injector due to mixing (see Figure 4). However, it does enable

an approximate concentration at t=0 to be determined. The HO_2 concentration exiting the injector was varied by changing the Hg lamp current, and thus its photon flux. Within experimental constraints, it was possible to vary the initial [HO_2] by up to a factor of four.

Figure 12 shows the corrected first order rate constant, k', as a function of aerosol surface area for HO_2 uptake to NH_4NO_3 aerosols at RH=30% for two initial HO_2 concentrations. The resulting uptake coefficients, obtained using the moving injector method, were γ_{HO2}=0.009±0.004 and γ_{HO2}=0.004±0.002 for [HO_2]=2.7×10^9 and 1.1×10^9 molecule cm^{-3}, respectively. HO_2 mass accommodation values were also determined for Cu(II)-doped $(NH_4)_2SO_4$ aerosol at RH~56% by moving injector experiment at two initial HO_2 concentrations. These values were α_{HO2}=0.4±0.1 and α_{HO2}=0.6±0.2 for [HO_2]=2.8×10^9 and 1.0×10^9 molecule cm^{-3}, respectively. Although within the combined uncertainties, these results provide some evidence for a higher uptake coefficient and mass accommodation at lower [HO_2]. More extensive fixed injector experiments, as shown in Figure 13 for aqueous NaCl at RH=60%, demonstrate a similar trend with an increase in γ_{HO2} at lower [HO_2]. Reactive uptake coefficients were enhanced at the lower value of the initial [HO_2] by up to 80%, but varied with injector distance.

To further explore an [HO_2] dependence, γ_{HO2} values from individual experiments used to calculate mean values for aqueous $(NH_4)_2SO_4$ aerosol in Table 2 are shown in Figure 14 as a function of initial [HO_2]. There is a similar trend towards larger values of γ_{HO2} at lower HO_2 concentrations. This trend appears more apparent for 65-75% RH compared with 54%, although the higher RH experiments are associated with greater variability. As noted previously, all experiments using dry aerosols resulted in γ_{HO2} values below the detection limit defined by the wall loss variability in the absence of aerosols. Therefore, any trend in the value of the uptake coefficient with HO_2 concentration could not be determined. One possible explanation for the trends in HO_2 uptake observed in this work with HO_2 concentrations could be aerosol surface saturation effects similar to time dependence, as mentioned previously. Generally, higher HO_2 concentrations would lead to greater surface saturation and reduced uptake. However, these observations alone do not confirm this mechanism. We plan to use the

KM-SUB model to further investigate the HO_2 concentration dependence on the HO_2 uptake to aerosols to attempt to elucidate the reaction mechanisms involved.

3.6. Comparison of measured γ_{HO2} with literature values

Tables 1 and 2 summarize HO_2 reactive uptake coefficients reported in the literature for salt aerosols and the values obtained in this work using the moving injector method, respectively. There was no observable HO_2 uptake onto dry salt aerosols within the experimental detection limits (γ_{HO2}<0.004) in this work. In general, the γ_{HO2} values measured on dry salt aerosols determined in this work are significantly lower than some of the literature values. Several groups have measured HO_2 uptake onto dry NaCl salt films and dry aerosol particles[25]. Two of those studies reported uptake values less than γ_{HO2}<0.01 at low RH (≤ 20%), which were in agreement with γ_{HO2} values observed at all RH in this work.

The HO_2 mass accommodation values obtained in this work (α_{HO2}=0.26–0.64, mean α_{HO2}=0.4±0.3) were consistent with literature values obtained from HO_2 uptake onto Cu(II)-doped salt aerosols with α_{HO2} >0.2. However, the measurements presented here for HO_2 uptake onto aqueous salt aerosols in the absence of Cu(II) ions deviate most significantly from previous literature values. Few studies have quantitatively measured HO_2 uptake onto aqueous salt aerosols. Furthermore, there have been no reported γ_{HO2} values for aqueous salt films in coated wall experiments to our knowledge. Thornton and Abbatt[32] observed second-order kinetics for HO_2 uptake onto aqueous $(NH_4)_2SO_4$ aerosols at RH=42%, and reported an approximate uptake value of γ_{HO2}~0.1 by assuming first-order kinetics in the analysis of their data to enable comparison with other studies. The measurements in that study, which were performed for much higher $[HO_2]= 2.5 \times 10^{10} - 5 \times 10^{10}$ molecule cm^{-3} were found to be consistent with known aqueous chemistry involving second-order HO_2 self-reaction in bulk phase (i.e. Reactions (R1)-(R3)).

The HO_2 uptake coefficient obtained at much higher concentrations can be extrapolated to lower HO_2 concentrations using the currently understood aqueous chemistry of HO_2, as outlined by Thornton et al.[48] For conditions that resemble this work for $(NH_4)_2SO_4$ aerosols, namely 293 K, α_{HO2} = 0.4, $[HO_2]$ ~10^9 molecule cm^{-3} and

assuming an aerosol pH=5, an extrapolated value γ_{HO2}~0.002 was calculated using Equation (7) in Thornton et al.[48] It should be noted that this calculation is extremely sensitive to aerosol pH due to the pH-dependent HO_2 solubility. For example, the calculated uptake coefficient for NaCl aerosols at pH~7 becomes γ_{HO2}~0.12. Aerosol pH can be calculated from the composition of the solutions used to generate the aerosols and RH in the aerosol flow tube assuming no gas-phase species impact the aerosol pH. However, it is not possible to directly measure the exact pH of the aerosols in the experiments to confirm that experiments were conducted with aerosols of similar pH. Therefore, assuming that the aqueous chemistry of HO_2 is solely described by Reactions (R1)-(R3), it may be possible that the differences in the measured uptake coefficients are due to the aerosols in different studies having a slightly different pH.

In contrast to Thornton and Abbatt[32], Taketani et al.[25] observed first-order HO_2 uptake kinetics onto aqueous salt aerosols similar to other studies. In our work, the data was fitted assuming first-order kinetics as this gave a slightly better goodness of fit (R^2 value) than assuming second-order kinetics. The negative dependence of HO_2 uptake on HO_2 concentration observed in this work appears to be in disagreement with second-order kinetics of aerosol-phase HO_2 self reaction. The γ_{HO2} values from Taketani et al [25] are at least an order of magnitude higher than values obtained in this work, i.e. in the range γ_{HO2}=0.09-0.19 for aqueous NaCl and $(NH_4)_2SO_4$ aerosols for a range of RH values of 45-75%. Taketani et al.[25] conducted HO_2 uptake experiments using a similar reaction setup to this work, including similar reaction flow tube dimensions, method of aerosol generation, and HO_2 detection by the FAGE technique. There are a few notable differences between experimental conditions in this work and Taketani et al.[25] that potentially may have led to disagreements in measured γ_{HO2} values as described below.

The majority of experiments in this work were conducted with N_2 as the bath gas containing a small impurity of O_2 to rapidly generate the HO_2 from H atoms. Nitrogen was used to avoid production of high concentrations of ozone (>1 ppm) to minimize any gas-phase secondary chemistry or aerosol modification. Taketani et al.[25] used air as a bath gas for all flows. However, some experiments were performed in air in this work to ensure there was no difference in HO_2 uptake due to different bath gases. For example, the HO_2 uptake onto aqueous $(NH_4)_2SO_4$ at RH=55% was measured in air with a value of γ_{HO2}=0.004 ± 0.002, which is consistent with the value obtained in N_2.

The HO_2 mass accommodation coefficient measured in air (α_{HO2}= 0.40±0.1) was also consistent with that measured in N_2.

Uptake experiments were conducted in Taketani et al.[25] at lower HO_2 concentrations and for shorter reaction times to determine γ_{HO2} compared to this work. The [HO_2] used in Taketani et al.[25] was ~2-10 times lower than the range of values used in this work. As discussed earlier, we have shown some evidence that the uptake coefficient exhibited a negative dependence on [HO_2], but this cannot explain the significant differences in uptake values between this work and Taketani et al.[25] The moving injector experiments in this work were conducted over reaction times in the range of approximately 11-20 s, while Taketani et al.[25] measured uptake values over reaction times of ~5-11 s corresponding to the mixing region in this work. We found that the γ_{HO2} values obtained from the fixed injector experiments increased with shorter reaction times. These uptake coefficients are cumulative average values that contain a contribution from relatively high rates of HO_2 loss owing to dilution after injection and possible fast uptake onto fresh aerosols. A combination of time and HO_2 concentration dependences on the value of γ_{HO2} may explain some of the discrepancies with Taketani et al.[25] However, the HO_2 uptake in this work was never measured as high as γ_{HO2}~0.1 for aqueous aerosol in the absence of Cu(II) ions as was consistently observed by Taketani et al.[25]

Finally, it is worth noting the significant increase in the uptake coefficient we found in the presence of even very small concentrations of transition metal ions (TMI). Inconsistent results were sometimes obtained, giving higher values of γ_{HO2} that were not reported here. Upon quantitative analysis of the solutions used to generate the aerosols using ICP-MS, elevated concentrations of TMI were observed. In some cases, we were able to diagnose the source of the TMI as being from metallic parts of the apparatus, for example the impactor. Aged solutions were also sometimes found to contain elevated levels of TMI. We have analyzed every solution used for TMI concentrations using ICP-MS, and have discarded any data where these values were elevated. We plan to use the KM_SUB model to further investigate [HO_2], RH, time-dependent and TMI effects on the value of γ_{HO2} for comparison with the experimental data obtained in this work and previously reported in the literature.

4. Atmospheric Implications

The potential impact of HO_2 heterogeneous uptake on atmospheric HO_2 concentrations based on observations from this work was examined using a simple box model which had previously been used to calculate OH and HO_2 levels for comparison with field data measured at the Cape Verde Atmospheric Observatory[15]. A constant HO_2 uptake coefficient γ_{HO2}=0.01 was used for aqueous salt aerosols, where all aerosols were assumed to be in aqueous phase. For a typical daytime HO_2 concentration[14] of [HO_2] ~3 × 10^8 molecule cm^{-3}, HO_2 uptake to aerosols only lead to a decrease of [HO_2] of ~2% for this marine environment assuming a typical atmospheric aerosol surface concentration of 1 × 10^{-6} cm^2cm^{-3}.[15] As discussed in the Introduction, significantly higher uptake coefficient values, in some cases as high as γ_{HO2}=1, had been used in box models in an attempt to explain the "missing HO_2 sink" that was needed during some field campaigns to bring modeled HO_2 into line with field measurements. This was particularly the case for the marine environment, where the importance of halogen chemistry as a sink for HO_2 had not been realised. The results from this study suggest that in the absence of transition metal ions the heterogeneous uptake to aqueous salt aerosols is not a significant sink for HO_2.

However, there may be high enough concentrations of transition metal ions, such as copper and iron, in atmospheric aerosols for the uptake coefficient to be close to the mass accommodation coefficient[32, 33, 36, 49]. For example, Taketani et al.[33] recently measured high HO_2 uptake coefficients (γ_{HO2}=0.09-0.4) for aerosols produced from water extracts of ambient particle samples collected in China. In this work, the sampled particles contained Cu and Fe concentrations between 10-80 ng m^{-3} and 1.7-11.6 μg m^{-3}, respectively. Their calculations showed that only a small fraction of the transition metal measured in the aerosol phase needed to be in free ion form to explain the high HO_2 uptake, therefore indicating that most of the Cu and Fe in extracts were not in free ion form. It has been suggested that Cu and other TMI in atmospheric aerosols may be bound in highly organic rich matrixes and can form complexes with hydroxide or sulfate ions, where the measured metal concentration as well as the free ion fractions in the air may be highly variable from particle to particle[48]. These factors would reduce the HO_2 uptake coefficient associated with TMI chemistry as well as introduce variability

in HO_2 uptake onto ambient aerosols, as observed by Taketani et al.[33] Other factors that may contribute to uncertainties in the atmospherically relevant HO_2 uptake coefficient also arise due to inability to quantify the exact pH of atmospheric aerosols and the lack of HO_2 uptake data for organic aerosols, which are prevalent in the atmosphere. Therefore, further studies are required covering a wide range of atmospherically relevant conditions in order to determine a set of values for the HO_2 uptake coefficient that should be used in atmospheric models.

5. Conclusions.

HO_2 uptake coefficients have been measured onto submicron aerosols using an aerosol flow tube coupled with a highly sensitive FAGE detection system capable of measuring HO_2 at ambient levels. Uptake coefficients were below detection (γ_{HO2}<0.004) for dry (effloresced) salts (NaCl and $(NH_4)_2SO_4$) and were in the range γ_{HO2}=0.003-0.016 for aqueous (deliquesced) salts (NaCl, $(NH_4)_2SO_4$ and NH_4NO_3). No detectable relative humidity dependence was observed for the effloresced or deliquesced salts. The mass accommodation coefficient was found to be α_{HO2}=0.4±0.3 using $(NH_4)_2SO_4$ aerosols doped with Cu(II) ions. Although the value of α_{HO2} was in agreement with the literature, the measured values of γ_{HO2} for salt aerosols were significantly smaller than some of the values currently in the literature. For example, Taketani et al.[25] measured uptake coefficients approximately an order of magnitude greater than our results for aqueous salt particles using a similar method to this work. Due to this disagreement, extensive quality control measures were performed to provide additional confidence in the measurements. For example, we have verified that the correct aerosol surface area was being measured, that the flows were well mixed and that the atomizer solutions were not contaminated with trace metals, in particular transition metal ions.

The measurements presented in this work provide some evidence that reaction time and HO_2 concentration dependences may be responsible for some of the disagreements of values from this work with those from Taketani et al.[25], as well as the variability of the uptake values in the literature. Both mass accommodation and HO_2 uptake values showed similar negative trends with increasing time and [HO_2]. One possible mechanism that was proposed to explain these dependences is saturation of the

aerosol surface with increasing time and [HO_2]. Detailed kinetic modeling is required to evaluate the kinetic processes that control HO_2 uptake to aerosols. The KM-SUB numerical model[47] is currently being adapted to incorporate the uptake of HO_2 radicals onto aerosols. Future work will explore the dependence of γ_{HO2} upon a wide range of experimental parameters for comparison with experimental measurements to determine the optimum values to be recommended for inclusion into atmospheric models.

Acknowledgements

This work was supported by the National Environment Research Council under grant NE/F020651/1. PSJM is grateful to NERC for the award of a studentship. LJW, BB and DEH are also grateful to the NERC funded National Centre for Atmospheric Science for ongoing support.

References

1. W. H. Brune, D. Tan, I. F. Faloona, L. Jaegle, D. J. Jacob, B. G. Heikes, J. Snow, Y. Kondo, R. Shetter, G. W. Sachse, B. Anderson, G. L. Gregory, S. Vay, H. B. Singh, D. D. Davis, J. H. Crawford and D. R. Blake, *Geophysical Research Letters*, 1999, **26**, 3077-3080.
2. C. A. Cantrell, R. E. Shetter, T. M. Gilpin and J. G. Calvert, *Journal of Geophysical Research-Atmospheres*, 1996, **101**, 14643-14652.
3. N. Carslaw, D. J. Creasey, D. E. Heard, P. J. Jacobs, J. D. Lee, A. C. Lewis, J. B. McQuaid, M. J. Pilling, S. Bauguitte, S. A. Penkett, P. S. Monks and G. Salisbury, *Journal of Geophysical Research-Atmospheres*, 2002, **107**.
4. N. Carslaw, D. J. Creasey, D. E. Heard, A. C. Lewis, J. B. McQuaid, M. J. Pilling, P. S. Monks, B. J. Bandy and S. A. Penkett, *Journal of Geophysical Research-Atmospheres*, 1999, **104**, 30241-30255.
5. A. L. Haggerstone, L. J. Carpenter, N. Carslaw and G. McFiggans, *Journal of Geophysical Research-Atmospheres*, 2005, **110**.
6. L. Jaegle, D. J. Jacob, W. H. Brune, I. Faloona, D. Tan, B. G. Heikes, Y. Kondo, G. W. Sachse, B. Anderson, G. L. Gregory, H. B. Singh, R. Pueschel, G. Ferry, D. R. Blake and R. E. Shetter, *Journal of Geophysical Research-Atmospheres*, 2000, **105**, 3877-3892.
7. Y. Kanaya, R. Cao, S. Kato, Y. Miyakawa, Y. Kajii, H. Tanimoto, Y. Yokouchi, M. Mochida, K. Kawamura and H. Akimoto, *Journal of Geophysical Research-Atmospheres*, 2007, **112**.
8. Y. Kanaya, Y. Sadanaga, J. Matsumoto, U. K. Sharma, J. Hirokawa, Y. Kajii and H. Akimoto, *Journal of Geophysical Research-Atmospheres*, 2000, **105**, 24205-24222.
9. J. Mao, D. J. Jacob, M. J. Evans, J. R. Olson, X. Ren, W. H. Brune, J. M. St Clair, J. D. Crounse, K. M. Spencer, M. R. Beaver, P. O. Wennberg, M. J. Cubison, J. L. Jimenez, A. Fried, P. Weibring, J. G. Walega, S. R. Hall, A. J. Weinheimer, R. C. Cohen, G. Chen, J. H. Crawford, C. McNaughton, A. D. Clarke, L. Jaegle, J. A. Fisher, R. M. Yantosca, P. Le Sager and C. Carouge, *Atmospheric Chemistry and Physics*, 2010, **10**, 5823-5838.
10. S. C. Smith, J. D. Lee, W. J. Bloss, G. P. Johnson, T. Ingham and D. E. Heard, *Atmospheric Chemistry and Physics*, 2006, **6**, 1435-1453.
11. R. Sommariva, W. J. Bloss, N. Brough, N. Carslaw, M. Flynn, A. L. Haggerstone, D. E. Heard, J. R. Hopkins, J. D. Lee, A. C. Lewis, G. McFiggans, P. S. Monks, S. A. Penkett, M. J. Pilling, J. M. C. Plane, K. A. Read, A. Saiz-Lopez, A. R. Rickard and P. I. Williams, *Atmospheric Chemistry and Physics*, 2006, **6**, 1135-1153.
12. R. Sommariva, A. L. Haggerstone, L. J. Carpenter, N. Carslaw, D. J. Creasey, D. E. Heard, J. D. Lee, A. C. Lewis, M. J. Pilling and J. Zador, *Atmospheric Chemistry and Physics*, 2004, **4**, 839-856.
13. P. S. Stevens, J. H. Mather and W. H. Brune, *Journal of Geophysical Research-Atmospheres*, 1994, **99**, 3543-3557.
14. D. Stone, L. K. Whalley and D. E. Heard, *Chemical Society Reviews*, 2012, **41**, 6348-6404.
15. L. K. Whalley, K. L. Furneaux, A. Goddard, J. D. Lee, A. Mahajan, H. Oetjen, K. A. Read, N. Kaaden, L. J. Carpenter, A. C. Lewis, J. M. C. Plane, E. S. Saltzman, A. Wiedensohler and D. E. Heard, *Atmospheric Chemistry and Physics*, 2010, **10**, 1555-1576.
16. W. J. Bloss, J. D. Lee, G. P. Johnson, R. Sommariva, D. E. Heard, A. Saiz-Lopez, J. M. C. Plane, G. McFiggans, H. Coe, M. Flynn, P. Williams, A. R. Rickard and Z. L. Fleming, *Geophysical Research Letters*, 2005, **32**.
17. Y. Kanaya, Y. Yokouchi, J. Matsumoto, K. Nakamura, S. Kato, H. Tanimoto, H. Furutani, K. Toyota and H. Akimoto, *Geophysical Research Letters*, 2002, **29**.

18. H. L. Macintyre and M. J. Evans, *Atmospheric Chemistry and Physics*, 2011, **11**, 10965-10974.
19. J. F. Lamarque, J. T. Kiehl, P. G. Hess, W. D. Collins, L. K. Emmons, P. Ginoux, C. Luo and X. X. Tie, *Geophysical Research Letters*, 2005, **32**.
20. R. V. Martin, D. J. Jacob, R. M. Yantosca, M. Chin and P. Ginoux, *Journal of Geophysical Research-Atmospheres*, 2003, **108**.
21. X. Tie, G. Brasseur, L. Emmons, L. Horowitz and D. Kinnison, *Journal of Geophysical Research-Atmospheres*, 2001, **106**, 22931-22964.
22. D. J. Jacob, *Atmospheric Environment*, 2000, **34**, 2131-2159.
23. M. Mozurkewich, P. H. McMurry, A. Gupta and J. G. Calvert, *Journal of Geophysical Research-Atmospheres*, 1987, **92**, 4163-4170.
24. P. Davidovits, C. E. Kolb, L. R. Williams, J. T. Jayne and D. R. Worsnop, *Chemical Reviews*, 2006, **106**, 1323-1354.
25. F. Taketani, Y. Kanaya and H. Akimoto, *Journal of Physical Chemistry A*, 2008, **112**, 2370-2377.
26. J. A. Thornton and J. P. D. Abbatt, *Journal of Physical Chemistry A*, 2005, **109**, 10004-10012.
27. Y. M. Gershenzon, V. M. Grigorieva, A. V. Ivanov and R. G. Remorov, *Faraday Discussions*, 1995, **100**, 83-100.
28. E. Loukhovitskaya, Y. Bedjanian, I. Morozov and G. Le Bras, *Physical Chemistry Chemical Physics*, 2009, **11**, 7896-7905.
29. R. G. Remorov, Y. M. Gershenzon, L. T. Molina and M. J. Molina, *Journal of Physical Chemistry A*, 2002, **106**, 4558-4565.
30. J. P. D. Abbatt, A. K. Y. Lee and J. A. Thornton, *Chemical Society Reviews*, 2012, **41**, 6555-6581.
31. F. Taketani, Y. Kanaya and H. Akimoto, *Atmospheric Environment*, 2009, **43**, 1660-1665.
32. J. Thornton and J. P. D. Abbatt, *Journal of Geophysical Research-Atmospheres*, 2005, **110**.
33. F. Taketani, Y. Kanaya, P. Pochanart, Y. Liu, J. Li, K. Okuzawa, K. Kawamura, Z. Wang and H. Akimoto, *Atmospheric Chemistry and Physics*, 2012, **12**, 11907-11916.
34. D. E. Heard, *Annual Review of Physical Chemistry*, 2006, **57**, 191-216.
35. D. E. Heard and M. J. Pilling, *Chemical Reviews*, 2003, **103**, 5163-5198.
36. J. Mao, S. Fan, D. J. Jacob and K. R. Travis, *Atmospheric Chemistry and Physics*, 2013, **13**, 509-519.
37. D. J. Cziczo and J. P. D. Abbatt, *Journal of Geophysical Research-Atmospheres*, 1999, **104**, 13781-13790.
38. D. J. Cziczo and J. P. D. Abbatt, *Journal of Physical Chemistry A*, 2000, **104**, 2038-2047.
39. D. J. Creasey, P. A. Halford-Maw, D. E. Heard, J. E. Spence and B. J. Whitaker, *Review of Scientific Instruments*, 1998, **69**, 4068-4073.
40. L. K. Whalley, K. L. Furneaux, T. Gravestock, H. M. Atkinson, C. S. E. Bale, T. Ingham, W. J. Bloss and D. E. Heard, *Journal of Atmospheric Chemistry*, 2007, **58**, 19-39.
41. R. Commane, C. F. A. Floquet, T. Ingham, D. Stone, M. J. Evans and D. E. Heard, *Atmospheric Chemistry and Physics*, 2010, **10**, 8783-8801.
42. L. F. Keyser, *Journal of Physical Chemistry*, 1984, **88**, 4750-4758.
43. R. L. Brown, *Journal of Research of the National Bureau of Standards*, 1978, **83**, 1-8.
44. N. A. S. Fuchs, A. G., 1970.
45. A. S. Wexler and S. L. Clegg, *Journal of Geophysical Research-Atmospheres*, 2002, **107**.
46. M. Ammann and U. Poschl, *Atmospheric Chemistry and Physics*, 2007, **7**, 6025-6045.
47. M. Shiraiwa, C. Pfrang and U. Poeschl, *Atmospheric Chemistry and Physics*, 2010, **10**, 3673-3691.

48. J. A. Thornton, L. Jaegle and V. F. McNeill, *Journal of Geophysical Research-Atmospheres*, 2008, **113**.
49. H. B. Ross and K. J. Noone, *Journal of Atmospheric Chemistry*, 1991, **12**, 121-136.

Table 1. Uptake coefficients for HO_2 onto inorganic salts from previous studies

Salt composition	Substrate Type and Phase	RH/ %	$[HO_2]$/ cm^{-3}	γ_{HO2}	Reference
$(NH_4)_2SO_4$	Dry aerosol	20	~10^8	0.04 ± 0.02	Taketani et al. (2008)[25]
	Dry aerosol	45	~10^8	0.05 ± 0.02	Taketani et al. (2008)[25]
NaCl	Dry film	0	4×10^9 - 3×10^{11}	0.016	Gershenzon et al. (2002)[27]
	Dry film	0	4×10^9 - 5×10^{11}	0.0117 ± 0.0008	Remorov et al. (2002)[29]
	Dry film	28	4×10^9 - 5×10^{11}	0.0102 ± 0.0008	Remorov et al. (2002)[29]
	Dry aerosol	20	~10^8	<0.01	Taketani et al. (2008)[25]
	Dry aerosol	45	~10^8	0.02 ± 0.01	Taketani et al. (2008)[25]
	Dry film	0	5×10^{11}	0.0018	Loukhovitskaya et al. (2009)[28]
$(NH_4)_2SO_4$	Aqueous aerosol	42	5×10^{10}	~0.1[a]	Thornton and Abbatt (2005)[26]
	Aqueous aerosol	45	~10^8	0.11 ± 0.03	Taketani et al. (2008)[25]
	Aqueous aerosol	55	~10^8	0.15 ± 0.03	Taketani et al. (2008)[25]
	Aqueous aerosol	65	~10^8	0.17 ± 0.04	Taketani et al. (2008)[25]
	Aqueous aerosol	75	~10^8	0.19 ± 0.04	Taketani et al. (2008)[25]
NaCl	Aqueous aerosol	53	~10^8	0.11 ± 0.03	Taketani et al. (2008)[25]
	Aqueous aerosol	63	~10^8	0.09 ± 0.02	Taketani et al. (2008)[25]
	Aqueous aerosol	75	~10^8	0.10 ± 0.02	Taketani et al. (2008)[25]
Cu(II)-doped $(NH_4)_2SO_4$	Aqueous aerosol	42	5×10^{10}	0.5 ± 0.1	Thornton and Abbatt (2005)[26]
	Aqueous aerosol	45	~10^8	0.53 ± 0.13	Taketani et al. (2008)[25]
Cu(II)-doped NaCl	Aqueous aerosol	53	~10^8	0.65 ± 0.17	Taketani et al. (2008)[25]
Cu(II)-doped NH_4HSO_4	Aqueous aerosol	75	10^8 - 10^9	0.40 ± 0.08	Mozurkewich et al. (1987)[23]

Table 2. Summary of γ_{HO2} values for salt aerosol particles for experiments at room temperature determined using the moving injector method. Errors represent the sum of random and systematic errors as discussed in the text. For the Cu(II)-doped $(NH4)_2SO_4$ aerosol γ_{HO2} represents the mass accommodation coefficient, α_{HO2}, with the uncertainty representing the range of values measured (over a range of conditions), rather than the uncertainty in any individual measurement ($1\sigma \leq 11\%$).

Aerosol Composition	RH / %	γ_{HO2}	Number of Determinations
Dry Salts			
$(NH_4)_2SO_4$	32 - 54	<0.004	4
NaCl	33 - 54	<0.004	3
Aqueous Salts			
Cu(II)-doped $(NH_4)_2SO_4$	53 - 65	0.4 ± 0.3	10
$(NH_4)_2SO_4$	55	0.003 ± 0.005	7
	65 - 75	0.01 ± 0.01	4
NaCl	54	0.016 ± 0.008	4
	67 - 76	0.01 ± 0.02	4
NH_4NO_3	29 - 70	0.005 ± 0.002	6

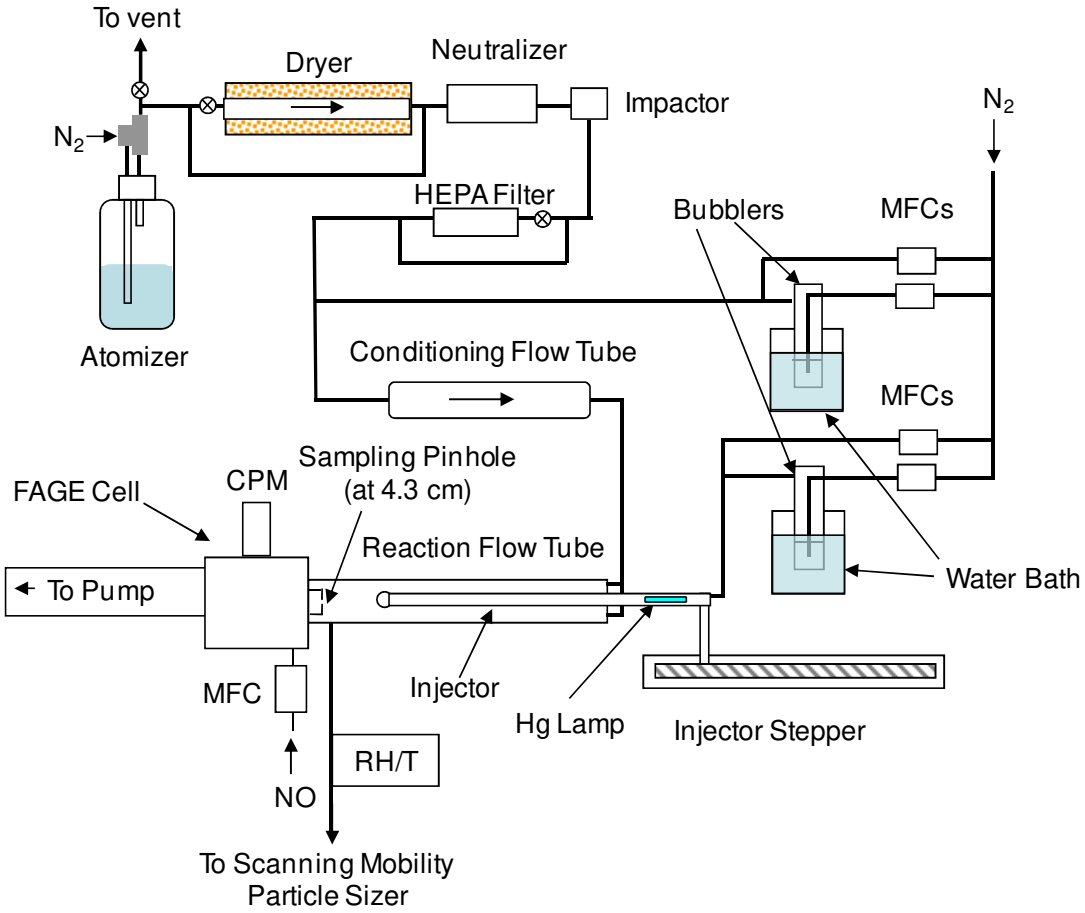

Figure 1. Schematic diagram of the aerosol flow tube system used to measure HO_2 uptake coefficients. Key: MFC - mass flow controller; RH/T - temperature and humidity probe; CPM - channel photomultiplier, FAGE - Fluorescence Assay by Gas Expansion; HEPA– High Efficiency Particulate Air.

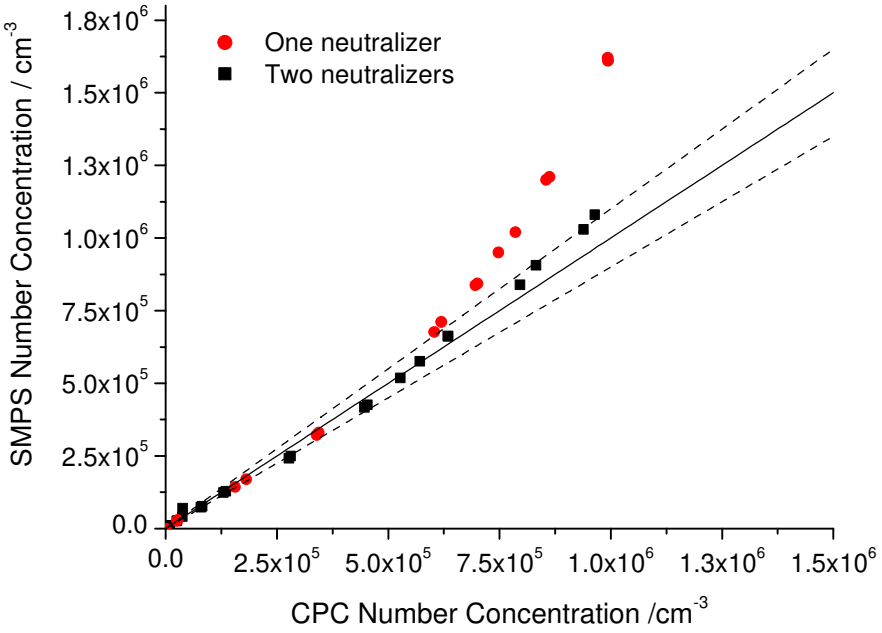

Figure 2. SMPS measured number concentration as a function of CPC measured number concentrations for aqueous NaCl particles with (black squares) and without (red circles) a second neutralizer in the aerosol flow. The black line is a linear least-squares fit to the black points and the dashed lines are a ±10% deviation from this fit.

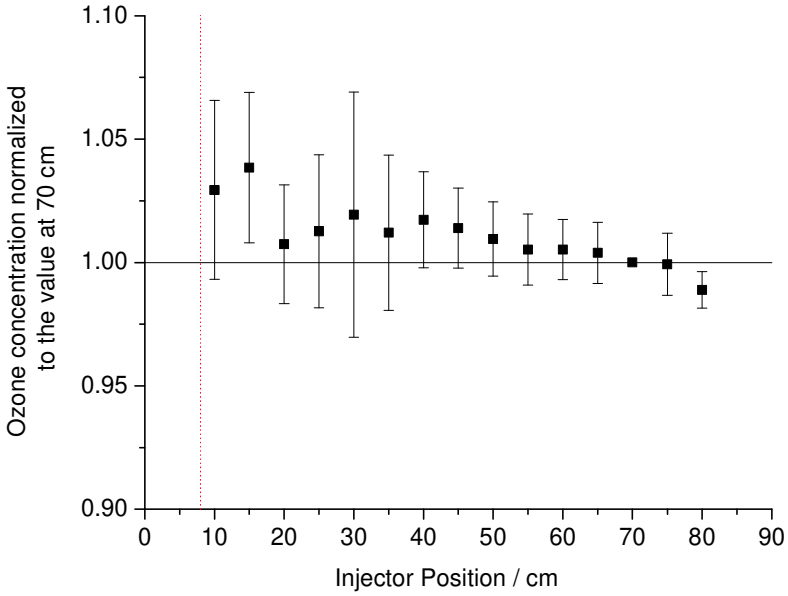

–

Figure 3. Ozone concentration profile as a function of distance along the flow tube, with the ozone sampling point positioned 8 cm from the FAGE pinhole (indicated by red vertical dotted line). The ozone concentration is normalized to the value measured at 70 cm.

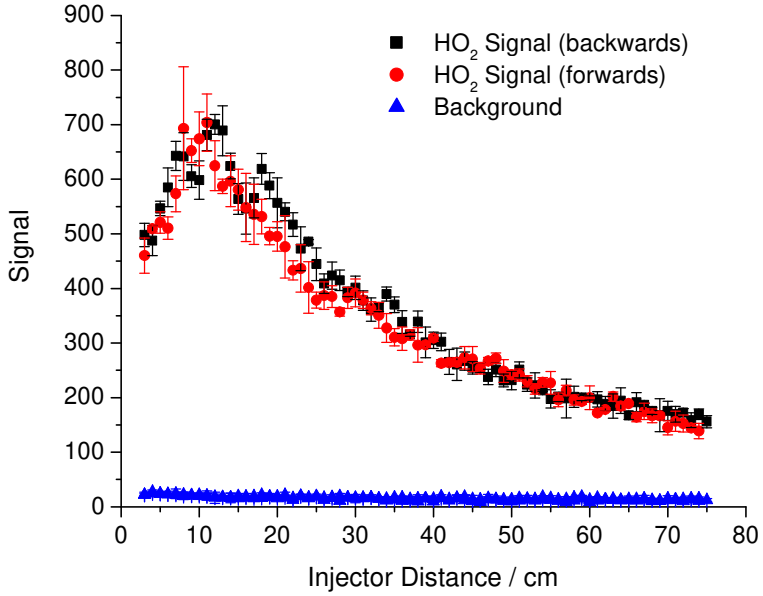

Figure 4: The FAGE signal as a function of injector distance in the presence of ammonium sulfate aerosols at a surface area concentration of 1.9×10^{10} cm^2 cm^{-3}. HO_2 signal (NO flow on) was measured while injector was moved away from the FAGE cell (black squares) and towards the FAGE cell (red circles). Background signal (NO flow off) was also measured (blue triangles).

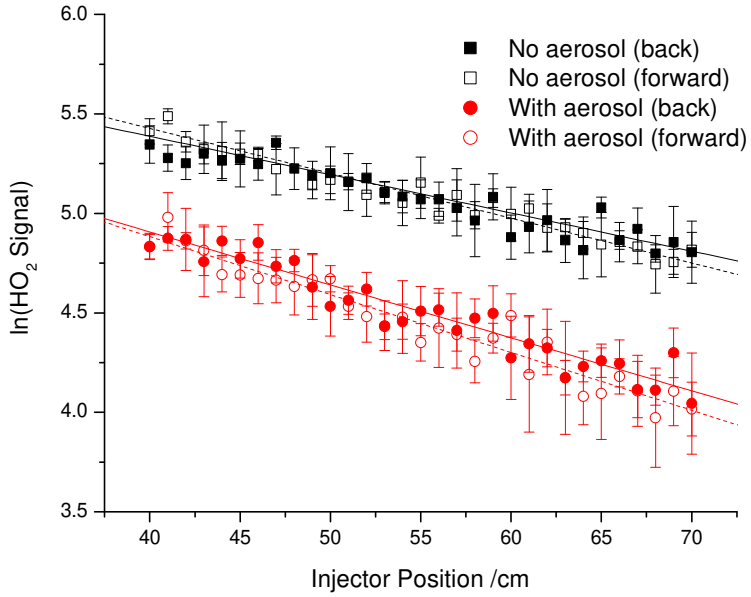

Figure 5. Natural log of the HO_2 signal as a function of injector distance for aqueous $(NH_4)_2SO_4$ aerosols at RH=54% in the absence (squares) and in the presence (circles) of aerosols for an aerosol surface area of S_a=5.9x10^{-4} cm^2 cm^{-3}. The signal was averaged for 3 s at each point, and error bars represent 1σ. Experiments with the injector stepped backwards and forwards relative to the FAGE cell are shown as solid and open symbols, respectively. The solid and dashed lines represent linear fits of Equation (2) to the backwards and forwards data, respectively.

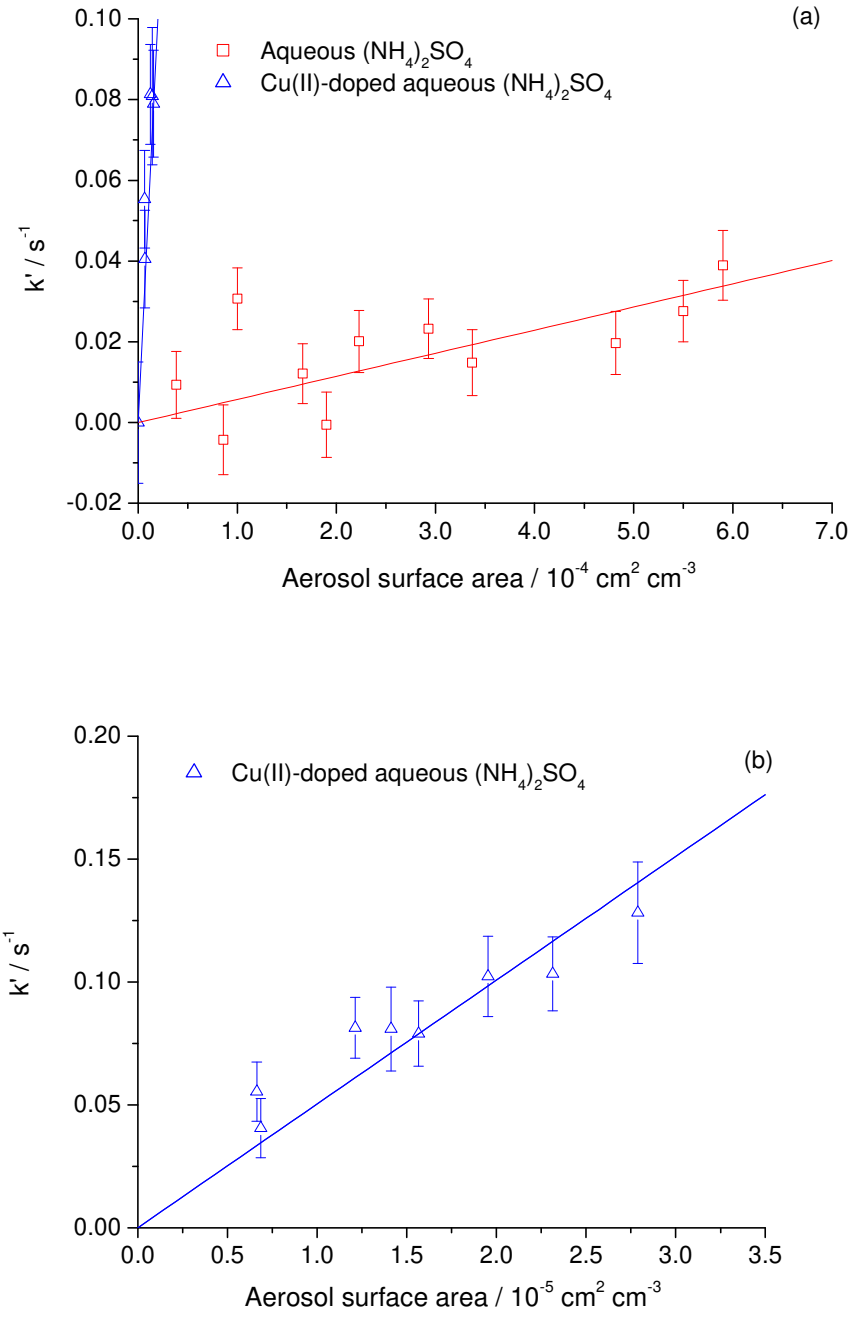

Figure 6. The first-order rate constants for HO_2 loss (k') following the Brown correction as a function of aerosol surface area for (a) aqueous $(NH_4)_2SO_4$ and Cu(II)-doped aqueous $(NH_4)_2SO_4$ aerosols at RH=54% and 55% respectively, (b) Cu(II)-doped aqueous $(NH_4)_2SO_4$ aerosols plotted alone. Error bars represent the 1σ propagated uncertainty for individual determinations of k'. The solid lines represent the error-weighted linear fits of Equation (3) to the data.

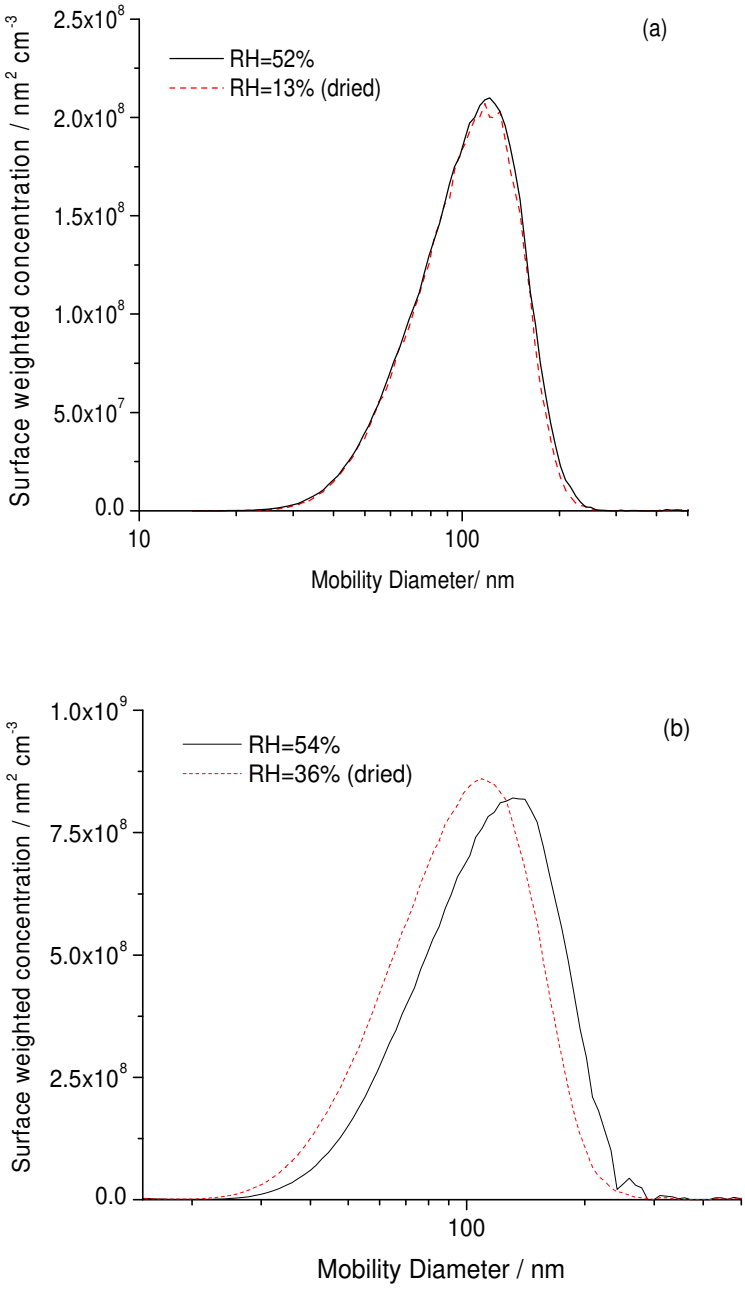

Figure 7. Surface area weighted size distributions: (a) Dry $(NH_4)_2SO_4$ aerosol particles at RH= 13% and 52%; (b) Aqueous $(NH_4)_2SO_4$ aerosols during uptake experiments at RH= 36 and 52% before and after the aerosol flow was dried to confirm the particle phase.

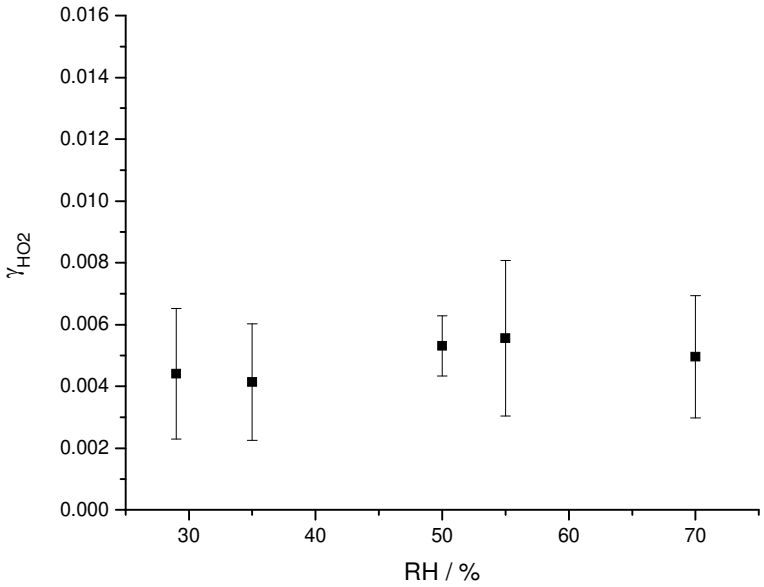

Figure 8. HO_2 uptake coefficients for aqueous NH_4NO_3 aerosols as a function of RH. Error bars represent 2σ of random errors and systematic errors.

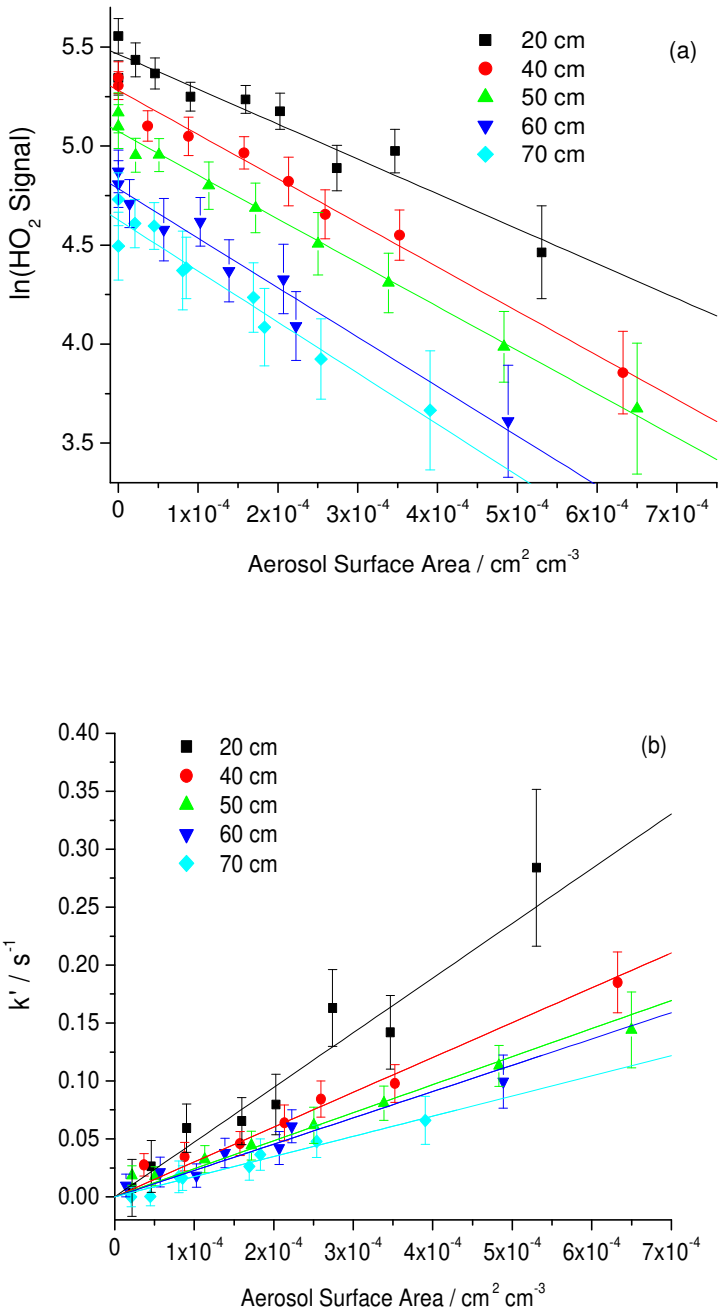

Figure 9. (a) Natural log of the HO_2 signal as a function of aerosol surface area for a range of fixed injector to HO_2 sampling distances. (b) Rate constants, k', following the Brown correction, as a function of aerosol surface area for a range of fixed injector to HO_2 sampling distances. Both plots are for aqueous $(NH_4)_2SO_4$ aerosols at RH=65% and error bars represent 1σ.

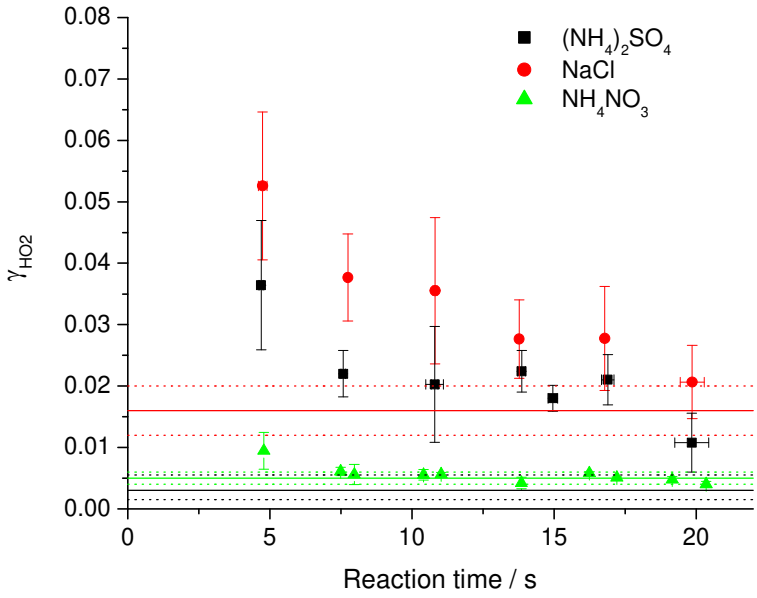

Figure 10. Reactive uptake coefficients, γ_{HO2}, onto aqueous salt aerosols as a function of reaction time for aqueous $(NH_4)_2SO_4$ at RH=54-75%, aqueous NH_4NO_3 aerosols at RH=20%, and aqueous NaCl aerosols at RH=60-65%. Error bars represent 1σ of the average values obtained from a number of repeated experiments for each reaction time. Solid lines represent the values of γ_{HO2} obtained during moving injector experiments for $(NH_4)_2SO_4$ (black) and NaCl (red), both at RH=54%, and NH_4NO_3 (green) averaged over the RH range of 29-70% (see Table 1 and Figure 7) plotted over the entire *x*-axis range for comparison. Dotted lines represent 1σ of these values.

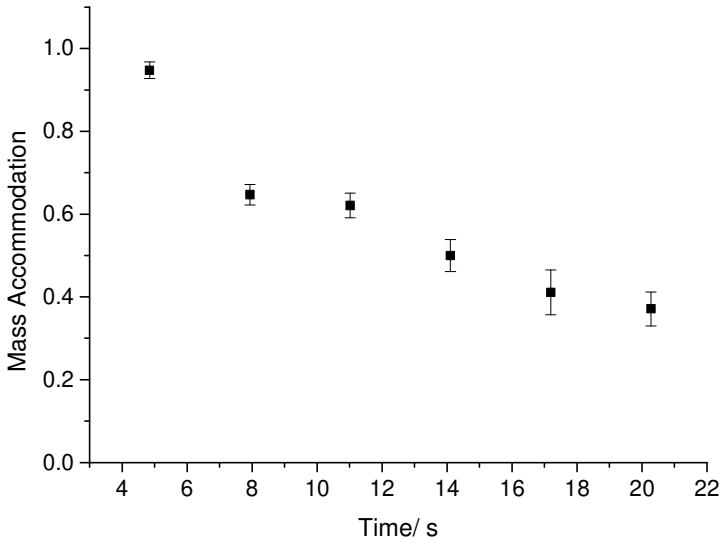

Figure 11. Mass accommodation coefficients for HO_2 at an initial concentration of 2.7×10^9 cm^{-3} onto Cu(II)-doped aqueous $(NH_4)_2SO_4$ aerosols as a function of reaction time.

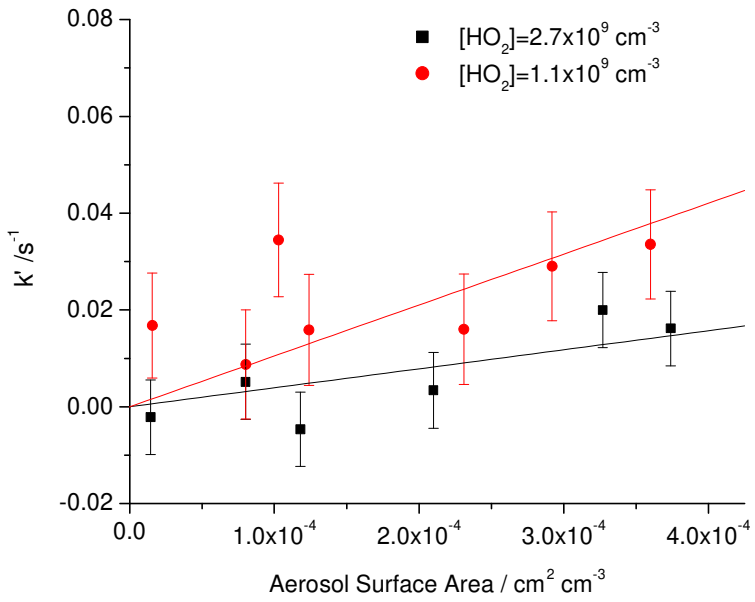

Figure 12. Corrected rate constants as a function of aerosol surface area for HO_2 uptake onto NH_4NO_3 aerosols at RH=30% for two initial HO_2 concentrations. Uptake coefficients calculated from fits to these data are γ_{HO2}=0.004±0.002 and γ_{HO2}=0.009±0.004 and for $[HO_2]$=1.1×10^9 molecule cm^{-3} and 2.7×10^9 molecule cm^{-3}, respectively. Error bars are 1σ of average values.

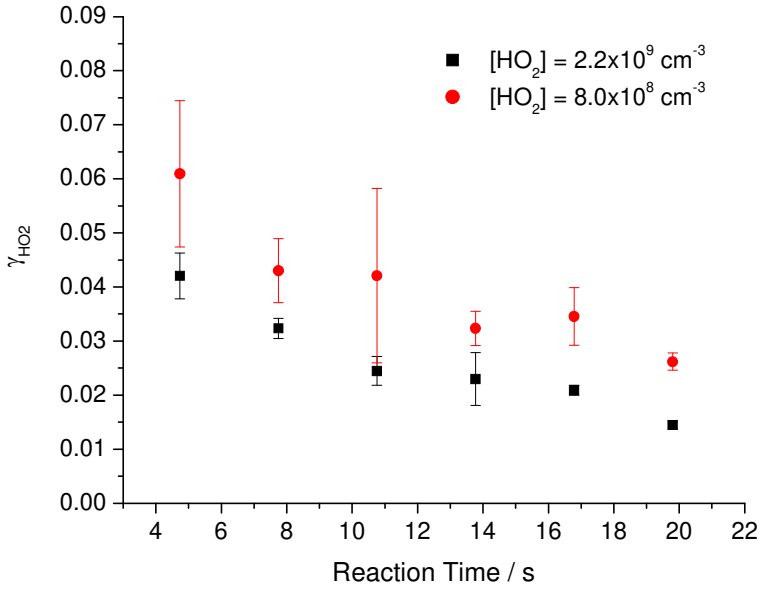

Figure 13. HO_2 uptake coefficients for aqueous NaCl aerosols at RH=60% as a function of reaction time from fixed injector experiments for two different initial HO_2 concentrations. Error bars are 1σ of average values.

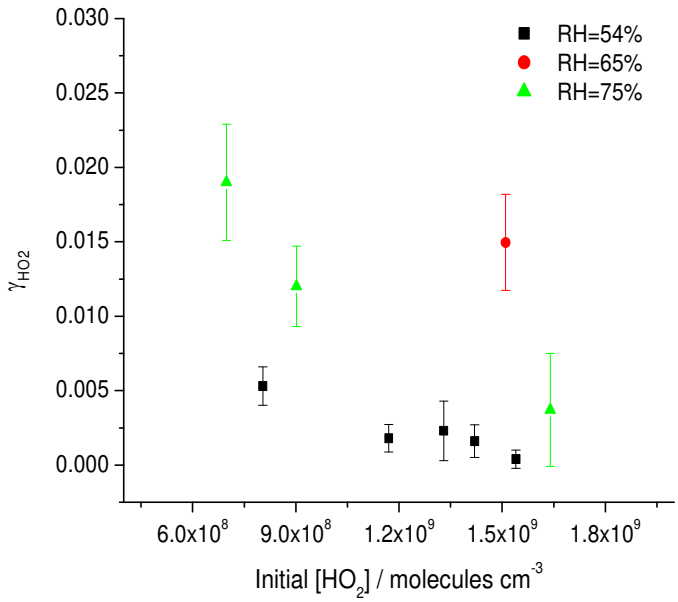

Figure 14. HO_2 uptake coefficients measured for aqueous $(NH_4)_2SO_4$ aerosols from individual moving injector experiments as a function of initial HO_2 concentration (t=0 s).